Satellight
Commission of the European Communities

DNMI

Fifth SATELLIGHT meeting, Sophia Antipolis November 27 - 28 1997

HIGH LATITUDE GLOBAL AND DIFFUSE RADIATION ESTIMATED FROM HELIOSAT-VERSIONS 7, 8, 9, and 10

by

Jan Asle Olseth and Arvid Skartveit

SATELLIGHT Programme JOR3-CT950041
First draft, November 1997

1. INTRODUCTION

Images taken by geostationary satellites are a valuable source to retrieve solar irradiance data with an almost continuous spatial coverage (Beyer et al., 1996). With increasing latitude, however, the accuracy of such retrievals declines due to the fact that geostationary satellites see the earth's surface at an increasingly unfavourable angle. This limitation is not shared by the sun-synchronous polar orbiting satellites, but the retrieval of solar irradiation from these satellites is hampered by their incomplete temporal coverage (Karlsson, 1994, 1996).

The present note compares some high latitude hourly ground observations with global radiation estimated from the geostationary satellite Meteosat. In addition to looking at the mean bias errors, our note focuses on how well frequency distributions of hourly global irradiance at the surface are reproduced by corresponding data retrieved from Meteosat data.

2. DATA

2.1 Meteosat/Heliosat data

The Heliosat procedure is described by Beyer et al. (1996). A measure of cloud cover is inferred from pixel counts in the VIS-channel (0.5 - 0.9 μm), and this measure is subsequently used to estimate surface global irradiance as a fraction of the irradiance under clear sky conditions. This procedure is carried out with one clear sky model, viz. the Kasten/Dumortier model with Linke turbidity coefficient 3.0 (Hammer 1996). As shown in Olseth & Skartveit (1997) the Kasten/Dumortier clear sky model and the McMaster model (Davies & McKay, 1989) with estimated climatological water vapor and turbidity as input, yield nearly identical cloud free global irradiances. These modelled values also agree nicely with observed cloud free irradiances at Bergen.

For each of our ground stations, global radiation data for 3 X 5 pixels centred around the ground pixel of the station, were estimated by the Heliosat procedure (versions 7, 8, 9, and 10) from Meteosat image acquisition each half hour for the period March 27. - December 31. 1995 (Hammer 1997). Based on these global radiation data, horizontal diffuse radiation is estimated by the original Skartveit & Olseth diffuse fraction model (1987). A recent modification of this model (Skartveit et al., 1997) is also used.

2.2 Ground truth data

Hourly global radiation measured by CM11 pyranometers are available from the nine stations (Table 1) plotted in Fig. 1. For three of the stations, hourly horizontal diffuse radiation data are available, measured by CM11 pyranometers with shading disk at Bergen and Gävle, and with shading ring at Ås. At Ås, misalignment of the shading ring was obvious for longer periods, and diffuse data from Ås are therefore not used here.

The difference with respect to time schedule of the various observations was approximately resolved as follows:

For stations run according to GMT, the ground observation for e. g. the hour 11^{00} - 12^{00} GMT is compared to a weighted average of Heliosat estimates at 10^{54}, 11^{24}, and 11^{54} GMT (with weights 0.25, 0.5, and 0.25). For Bergen, which is run according to Local Apparent Time (5°19'E), the ground observation for e. g. the hour 11^{30} - 12^{30} LAT is compared to the average of Heliosat estimates at 11^{24} and 11^{54} GMT. Note that the impact of the remaining minor time shifts is substantially reduced by

comparing averages and distributions of actual global / clear sky global irradiation rather than comparing individual pairs of corresponding hourly irradiations (see below).

3. RESULTS

3.1 The clear sky index

The clearness index for a given period is most commonly obtained by dividing the actual global irradiation H_g (observed or satellite-derived) by the extraterrestrial global irradiation H_{ex}. In the present note, we instead choose to divide by an "average" cloud-free irradiation H_o, and thus obtain the global clear sky index k_g:

$$\mathbf{k_g = H_g/H_o}. \qquad \textbf{(1)}$$

In a similar way the diffuse clear sky index k_d is defined by:

$$\mathbf{k_d = H_d/H_o}, \qquad \textbf{(2)}$$

where H_d is the actual diffuse irradiation on a horizontal surface.

Here H_g and H_d may be an observed irradiation or an irradiation derived from Meteosat data by the Heliosat Versions in question.

In this work all clear sky indices refers to the Kasten/Dumortier model with Linke turbidity factor 3.0. For brevity, global clear sky index is frequently referred to as clear sky index in this note.

3.2 Global irradiation

3.2.1 Hourly values

As an example, observed hourly global clear sky indices at 9 northern stations are plotted against their Heliosat Version 8 counterparts for snow free conditions (Fig. 2a). The average obs / satellite ratio ranges from 0.95 to 1.01 among the 9 stations. Fig. 2b) shows similar plots for possibly snow affected periods at two selected stations.

Frequency distributions of hourly clear sky indices (ground truth and satellite derived) at the 9 northern stations were formed for hours within solar elevation intervals. For solar elevations $\geq 10^\circ$, the satellite derived distributions (Figs. 3a-c) reasonably well reproduce the characteristic bimodal pattern of the distribution observed at the surface, which is characteristic of this climatic region (Skartveit & Olseth, 1992). It is noteworthy, however, that the cloudless mode of the surface observed distribution of clear sky index is somewhat broader than its Heliosat counterparts and slightly shifted towards lower values, in particular at low solar elevations. This is probably due to the fact that Heliosat is not explicitly designed to pick up the inherent variability (atmospheric absorption in particular) of cloud-free atmospheres.

For all solar elevations we then form

(1) the distribution of hourly global clear sky indices k_g observed at the ground, and
(2) the corresponding distribution of Heliosat (Versions 7, 8, or 9) cloud indices n.

We next plot "percentile match curves" as follows: the lowest k_g against the highest n, the second

lowest k_g against the second highest n, ..., the highest k_g against the lowest n. During the snow-free period, these curves vary only moderately between the 9 stations (Fig. 4a-c), and for the central 95% of the distributions, the ground truth curves are close to the following straight line:

$$\mathbf{k_g = 1 - n\ ,} \qquad \mathbf{(3)}$$

applied in Heliosat Versions 7 or 8 (Figs. 4a and b). For Version 9, however, some systematic deviations are seen between the line (3) and the ground truth observations (Fig. 4c).

For snow-free periods Figs. 5a-c) confirms this picture for all the 9 stations collectively. During the possibly snow affected periods, a significant number of high surface observed global clear sky indices is not reproduced by Heliosat Versions 7, 8, or 9 (Fig. 5a-c), most probably because Heliosat tend to interpret cloud free scenes with snow as partly cloud covered scenes.

Figs. 5a-c) also indicates that for high cloud indices, Heliosat Versions 7 and 9 tends to overestimate ground truth clearness index for high solar elevations. For low solar elevations Version 7 tends to underestimate the ground truth values while Version 9 shows only minor deviations from ground truth values. For low cloud indices (nearly cloud free) the ground truth / Heliosat 7, 8, or 9 ratio appears to be close to unity and more independent of solar elevation. It is noteworthy, however, that this solar elevation dependency of the observations vs. Heliosat conformity is least for Version 8 (Fig. 5b), in which case it is close to negligible for solar elevations > 20^o. This pattern is even seen for individual stations (not shown here). Moreover, Figs. 5a-c) show that the deviation between observations and Heliosat increases when possibly snow affected periods are considered.

3.2.2 Daily values

Observed daily clear sky indices and daily irradiations at all 9 stations are plotted against indices/irradiations retrieved from Meteosat data by Heliosat Versions 7, 8, and 9, both for snow free periods (Fig. 6a) and for possibly snow affected periods (Fig. 6b). A reasonable conformity between surface and satellite derived daily indices is seen for Versions 7 and 8, while Version 9 shows a marked positive mean bias. As an example we see that for 1168 snow free days the average ground truth / Heliosat irradiation ratio for Version 8 is 0.977, while the ratio is 1.106 for 98 possibly snow affected days.

3.2.3 Overall values

Figs. 7a-c) show satellite derived overall global clear sky indices at each of the 9 stations, plotted versus their surface observed counterparts. The spatial variation of ground observations is reasonably well reproduced by the Heliosat Versions 7 and 8 data, both within solar elevation intervals and for all solar elevations collectively. The observed clear sky index for all snow-free data (9 stations) is 0.640, while the satellite-derived counterparts are 0.639, 0.649, and 0.675 for Heliosat Versions 7, 8, and 9, respectively. (Table 2). The individual average clear sky indices for the 9 stations range from 0.567 to 0.720 for surface observed data, and from 0.557 to 0.727, from 0.570 to 0.735, and from 0.603 to 0.752, for satellite data derived from Versions 7, 8, and 9, respectively. The root-mean-square-deviation (surface vs satellite) of these individual averages are 0.010, 0.012, and 0.036 for Version 7, 8, and 9, respectively, i.e. only 6.5%, 7.8%, and 23.5% of the average inter-station range observed at the surface.

For the possibly snow affected data (6 stations) the satellite estimates show a significant underestimation (Fig. 7, Table 2). Fig. 2b) shows observed hourly global clear sky indices plotted against their Heliosat Version 8 counterparts for possibly snow affected conditions at the two stations

with largest underestimation in Table 2. As seen from Fig. 2b) there is a number of surface observed global clear sky indices in the range 2 - 3 at Landvik. The significance of these extremely high indices is, however, questionable since they occur at solar elevations < 10^o and may therefore be partly caused by other effects than high surface albedo. At Gävle, where the available data for possibly snow affected conditions are for higher solar elevations, we see that the ground truth exceed Heliosat by a more invariable amount than at Landvik.

3.3 Diffuse irradiation

3.3.1 Hourly values

Frequency distributions of hourly diffuse clear sky indices (ground truth and satellite derived) at the 2 northern stations with diffuse data were formed for hours with solar elevation within several intervals. A reasonable ground truth versus satellite agreement is seen (Fig. 8a-c), but the Heliosat Versions 7, 8, and 9 data covers a somewhat more narrow range than do the ground truth data. Moreover, the Heliosat data shows a more pronounced bimodal distribution pattern than what is seen in the ground truth data.

In Figs. 8a-c) the satellite derived diffuse irradiances were estimated using the original Skartveit & Olseth diffuse fraction model (Skartveit & Olseth, 1987). Calculations were also done by replacing the original diffuse fraction model with the modified version (Skartveit et al., 1997) for Heliosat Version 8, as an example. A comparison between Figs. 8d) and 8b) shows that the ground truth versus satellite agreement then increased significantly.

3.3.2 Daily values

Observed (ground truth) daily diffuse irradiations and diffuse clear sky indices are plotted against their counterparts derived from Heliosat Versions 7, 8, and 9, for the two northern stations with diffuse data (Fig. 9). For 293 snow free days the average ground truth / Heliosat ratio is 0.96 to 0.90 for the three Versions 7, 8, and 9, respectively, when the original Skartveit & Olseth diffuse fraction model (Skartveit & Olseth, 1987) is used for diffuse irradiance calculations.

By replacing the original model with the modified diffuse fraction model (Skartveit et al., 1997) the average ground truth / Heliosat Version 8 ratio increases from 0.94 to 0.97.

3.4 Frequency distributions of daily global and diffuse clear sky indices

According to Fig. 10 there is a nice agreement between frequency distribution of observed and Heliosat-derived daily clear sky indices, both for global and diffuse irradiation. As already seen for hourly values (Figs. 3a-c), the cloudless mode of the surface observed distribution of global clear sky index is somewhat broader than its Heliosat counterparts and slightly shifted towards lower values.

The figure also shows that by replacing the original Skartveit & Olseth diffuse fraction model (Skartveit & Olseth, 1987) with the modified diffuse fraction model (Skartveit et al., 1997) the ground truth versus satellite agreement increased significantly.

4. HELIOSAT VERSION 10

Recently, Meteosat data from a new Heliosat Version, namely Version 10, were received.

Frequency distributions of hourly clear sky indices (ground truth and satellite derived) at the 9 northern stations were formed for hours within solar elevation intervals for this new Version. For solar elevations $\geq 10^\circ$, Fig. 11 shows that the satellite derived distributions reasonably well reproduce the characteristic bimodal pattern of the distribution observed at the surface, in the same manner as for the three other Versions (Figs. 3a-c). Even for Version 10, however, the cloudless mode of the surface observed distribution of clear sky index is somewhat broader than its Heliosat counterparts and slightly shifted towards lower values, in particular at low solar elevations.

According to Fig. 11 there is also a nice agreement between frequency distribution of observed and Heliosat-derived daily global clear sky indices, just as for the three other Versions (Fig. 10). As for these three Versions, the cloudless mode of the surface observed distribution of global clear sky index is somewhat broader than its Heliosat counterpart and slightly shifted towards lower values.

We next plot "percentile match curves" as described in Chapter 3.2.1. For the central 95% of the distributions, the ground truth curves are close to the straight line $\mathbf{k_g = 1 - n}$ during the snow-free periods at the 9 stations collectively (Fig. 12), just as for Versions 7 and 8 (Figs. 5a-b). During the possibly snow affected periods, a significant number of high surface observed global clear sky indices is not reproduced by Heliosat Version 10 (Fig. 12), in the same manner as for the three other Versions (Figs. 5a-c).

As found for Version 8 (Fig. 5b), the solar elevation dependency of the observations vs. Heliosat Version 10 conformity is close to negligible for solar elevations > 20^o (Fig. 12).

The observed clear sky index for all snow-free data (9 stations) is 0.641, while the Heliosat Version 10 counterpart is 0.632 (Table 3). The individual average clear sky indices for the 9 stations range from 0.568 to 0.720 for surface observed data, and from 0.560 to 0.722 for Heliosat Version 10. The root-mean-square-deviation (surface vs satellite) of these individual averages is 0.014, i.e. only 8.6% of the average inter-station range observed at the surface.

As for the three other Versions (Table 2), the satellite estimates of Version 10 show a significant underestimation for the possibly snow affected data (Table 3).

5. CONCLUDING REMARKS

During the 280 days period March 27. - December 31. 1995, hourly observations of global irradiance at 9 high latitude ground stations show approximately the same frequency distribution as do corresponding data derived from Meteosat data by the Heliosat Version 7, 8, 9, and 10 models. The conformity between surface observations and Heliosat data was lowest for Version 9, while Versions 7, 8, and 10 gave similar results. Of these three last Versions, the solar elevation dependency of the conformity was weakest for Versions 8 and 10, and we therefore conclude that these two Versions fitted our data best.

The Heliosat Versions 7, 8, 9, and 10 data reasonably well reproduce the day to day variation in clear sky index, and even the observed spatial variation between 9 high latitude ground stations.

The occurrence of snow cover significantly reduces the agreement between surface observations and satellite derived data.

The hourly diffuse irradiances derived from Heliosat Versions 7, 8, 9, and 10 vary over a somewhat more narrow range than do the corresponding observed (ground truth) values at two northern stations,

and they even show a bimodal distribution pattern which is not seen with the ground truth data. This satellite vs. ground truth controversy is significantly reduced by replacing the original Skartveit & Olseth diffuse fraction model (Skartveit & Olseth, 1987) with a modified version (Skartveit et al., 1997). The remaining controversy may probably be completely resolved by introducing a diffuse fraction model which for given input parameters predicts a distribution of diffuse fraction rather than an expected average diffuse fraction. The average diffuse irradiance and the day to day variation of diffuse irradiation is, however, nicely reproduced by the Heliosat Versions 7, 8, 9, and 10 models.

Heliosat derives surface global irradiance from actual satellite counts along with corresponding cloud-free, respectively overcast, reference counts. The success of Heliosat critically depends on an adequate predetermination of these cloud-free/overcast reference counts. Our data demonstrate that a variable snow-cover strongly hampers an adequate predetermination of cloud-free reference counts, particularly in rural areas.

The overall conclusion is therefore:

- **At snow-free conditions Heliosat Versions 8 and 10 fitted our data best.**
- **The modified diffuse fraction model (Skartveit et al., 1997) improves the satellite derived diffuse irradiances significantly**

6. REFERENCES

H.G. Beyer, C. Costanzo and D. Heinemann (1996): Modifications of the Heliosat procedure for irradiance estimates from satellite images. Solar Energy **56**, 207 - 212.

J.A. Davies and D.C. McKay (1989): Evaluation of selected models for estimating solar radiation on horizontal surfaces. Solar Energy **43**, 152.

A. Hammer (1997): Satellite-derived global radiation data kindly submitted.

P. Ineichen (1997): Personal communication.

K.-G. Karlsson (1994): Satellite-estimated cloudiness from NOAA AVHRR data in the Nordic Area during 1993. SMHI Reports Meteorology and Climatology No. **66**.

K.-G. Karlsson (1996): Cloud classifications with the SCANDIA model. SMHI Reports Meteorology and Climatology No. **67**.

J.A. Olseth and A. Skartveit (1997): High latitude global and diffuse radiation estimated from Heliosat. First draft, May 1997. Fourth SATELLIGHT meeting, Oldenburg June 5-6, 1997.

A. Skartveit and J.A. Olseth (1987): A model for the diffuse fraction of hourly global radiation. Solar Energy **38**, 271 - 274.

A. Skartveit and J.A. Olseth (1992): The probability density and autocorrelation of short-term global and beam irradiance. Solar Energy **49**, 477 - 487.

A. Skartveit, J.A. Olseth and M.E. Tuft (1997): The potential for improvement of hourly diffuse fraction models. Submitted to Solar Energy, October 1997.

Table 1 Latitude (°N), longitude (°E), and elevation (m above mean sea level) for the 9 Scandinavian stations

Station	Lat. (°N)	Long. (°E)	Elev. (m asl.)
Landvik	58°19’	8°30’	6
Særheim	58°48’	5°08’	85
Ås	59°40’	10°51’	90
Bergen	60°24’	5°19’	45
Gävle	60°40’	17°10’	16
Apelsvoll	60°43’	10°51’	250
Løken	61°08’	9°08’	525
Fureneset	61°22’	5°35’	10
Kvithamar	63°27’	10°57’	30

Table 2a) Average clear sky indices (ratios between irradiation sums) observed at surface and derived from Meteosat by Heliosat Version 7 for the snow-free period and the period possibly affected by snow. (MBD = Heliosat Version 7 - Observed).

	No snow			″Snow″		
Station	**Obs.**	**V7**	**MBD**	**Obs.**	**V7**	**MBD**
Landvik	0.720	0.727	0.007	0.867	0.605	-0.222
Særheim	0.666	0.658	-0.008	-	-	-
Ås	0.643	0.660	0.017	0.724	0.696	-0.028
Bergen	0.596	0.603	0.007	-	-	-
Gävle	0.682	0.667	-0.015	0.716	0.585	-0.131
Apelsvoll	0.636	0.634	-0.002	0.706	0.641	-0.065
Løken	0.636	0.634	-0.002	0.689	0.645	-0.044
Fureneset	0.618	0.608	-0.010	-	-	-
Kvithamar	0.567	0.557	-0.010	0.650	0.600	-0.050
Overall	0.640	0.639	-0.001	0.725	0.629	-0.096

Table 2b) Same as Table 2a), but for Heliosat Version 8.

	No snow			″Snow″		
Station	**Obs.**	**V8**	**MBD**	**Obs.**	**V8**	**MBD**
Landvik	0.720	0.735	0.015	0.867	0.557	-0.310
Særheim	0.666	0.670	0.004	-	-	-
Ås	0.643	0.669	0.026	0.724	0.699	-0.025
Bergen	0.596	0.614	0.018	-	-	-
Gävle	0.682	0.676	-0.006	0.716	0.579	-0.137
Apelsvoll	0.636	0.642	0.006	0.706	0.649	-0.057
Løken	0.636	0.644	0.008	0.689	0.663	-0.026
Fureneset	0.618	0.619	0.001	-	-	-
Kvithamar	0.567	0.570	0.003	0.650	0.620	-0.030
Overall	0.640	0.649	0.009	0.725	0.628	-0.097

Table 2c) Same as Table 2a), but for Heliosat Version 9.

	No snow			″Snow″		
Station	**Obs.**	**V9**	**MBD**	**Obs.**	**V9**	**MBD**
Landvik	0.720	0.752	0.032	0.867	0.625	-0.242
Særheim	0.666	0.695	0.029	-	-	-
Ås	0.643	0.693	0.050	0.724	0.726	0.002
Bergen	0.596	0.643	0.047	-	-	-
Gävle	0.682	0.700	0.018	0.716	0.626	-0.090
Apelsvoll	0.636	0.669	0.033	0.706	0.683	-0.023
Løken	0.636	0.671	0.035	0.689	0.697	0.008
Fureneset	0.618	0.647	0.029	-	-	-
Kvithamar	0.567	0.603	0.036	0.650	0.660	0.010
Overall	0.640	0.675	0.035	0.725	0.670	-0.055

Table 3) Same as Table 2a), but for Heliosat Version 10.

	No snow			″Snow″		
Station	**Obs.**	**V10**	**MBD**	**Obs.**	**V10**	**MBD**
Landvik	0.720	0.722	0.002	0.867	0.541	-0.326
Særheim	0.667	0.649	-0.018	-	-	-
Ås	0.643	0.656	0.013	0.720	0.674	-0.046
Bergen	0.597	0.592	-0.005	-	-	-
Gävle	0.683	0.665	-0.018	0.728	0.570	-0.158
Apelsvoll	0.637	0.624	-0.013	0.703	0.608	-0.095
Løken	0.636	0.622	-0.013	0.691	0.571	-0.120
Fureneset	0.618	0.647	0.029	-	-	-
Kvithamar	0.568	0.560	-0.008	0.646	0.585	-0.102
Overall	0.641	0.632	-0.009	0.726	0.585	-0.141

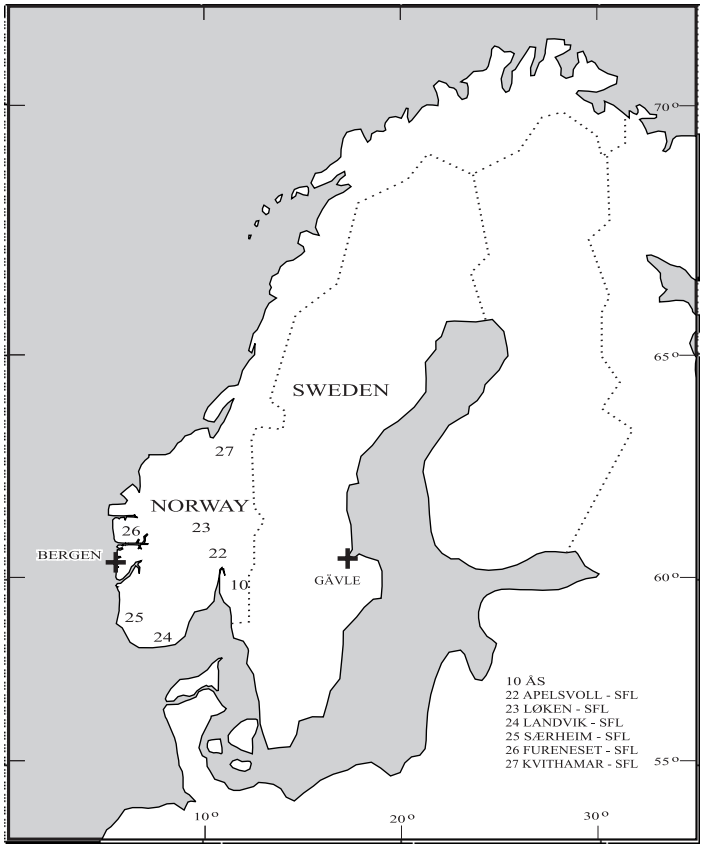

Fig. 1 Map with 9 ground stations plotted: Bergen (University of Bergen), Gävle (Royal Institute of Technology), Ås (Norwegian Agricultural University), and 6 stations run by the Norwegian Crop Research Institute (SFL).

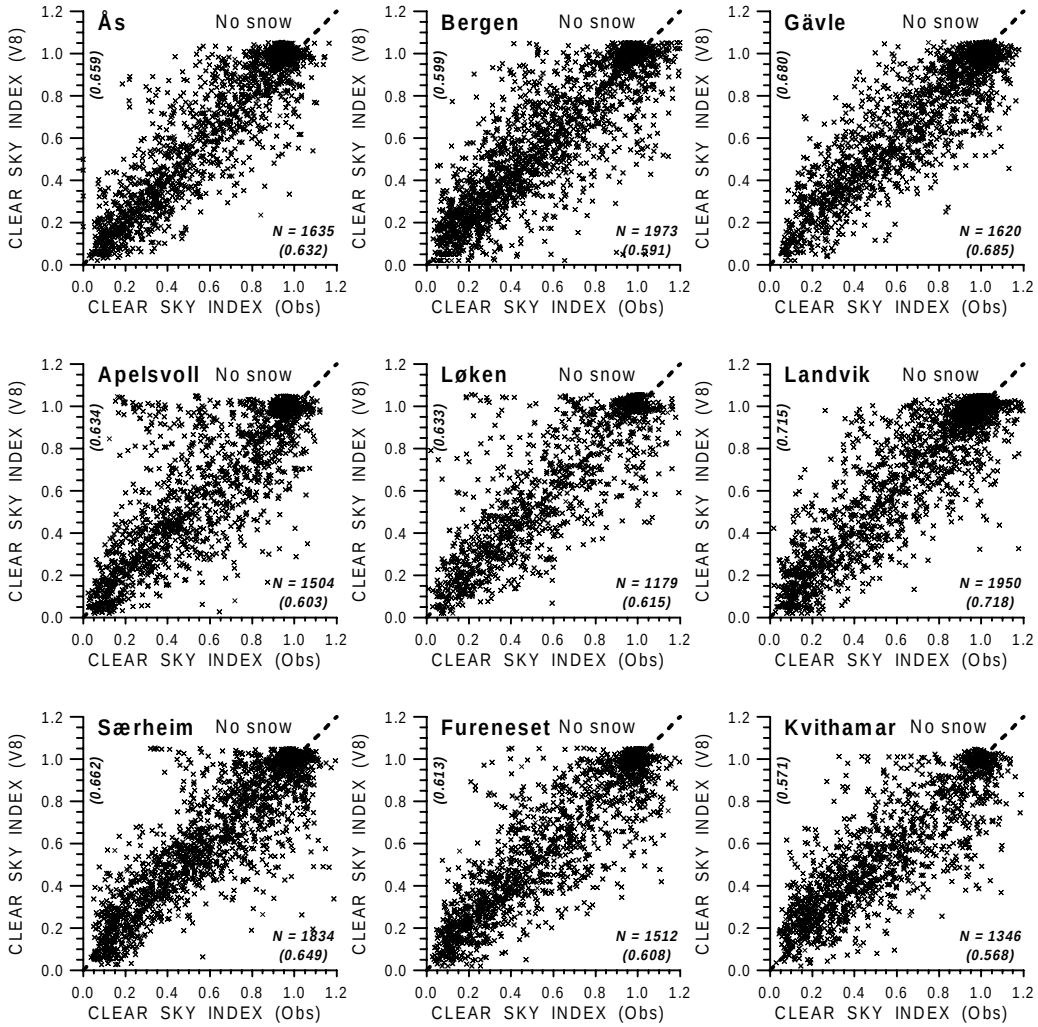

Fig. 2a) Observed vs modelled (Heliosat Version 8) hourly global clear sky index for the snow free periods at 9 northern stations. The number of hours (N) together with observed and modelled average indices (in parentheses along the axes) are also given.

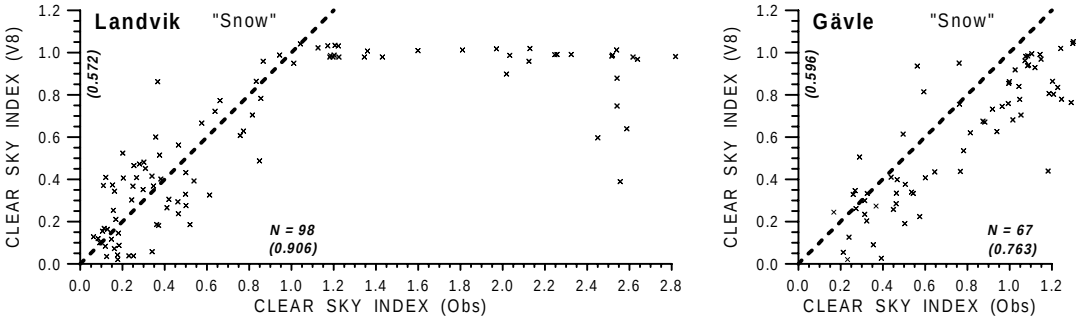

Fig. 2b) Same as Fig. 2a), but for possibly snow affected periods at 2 northern stations.

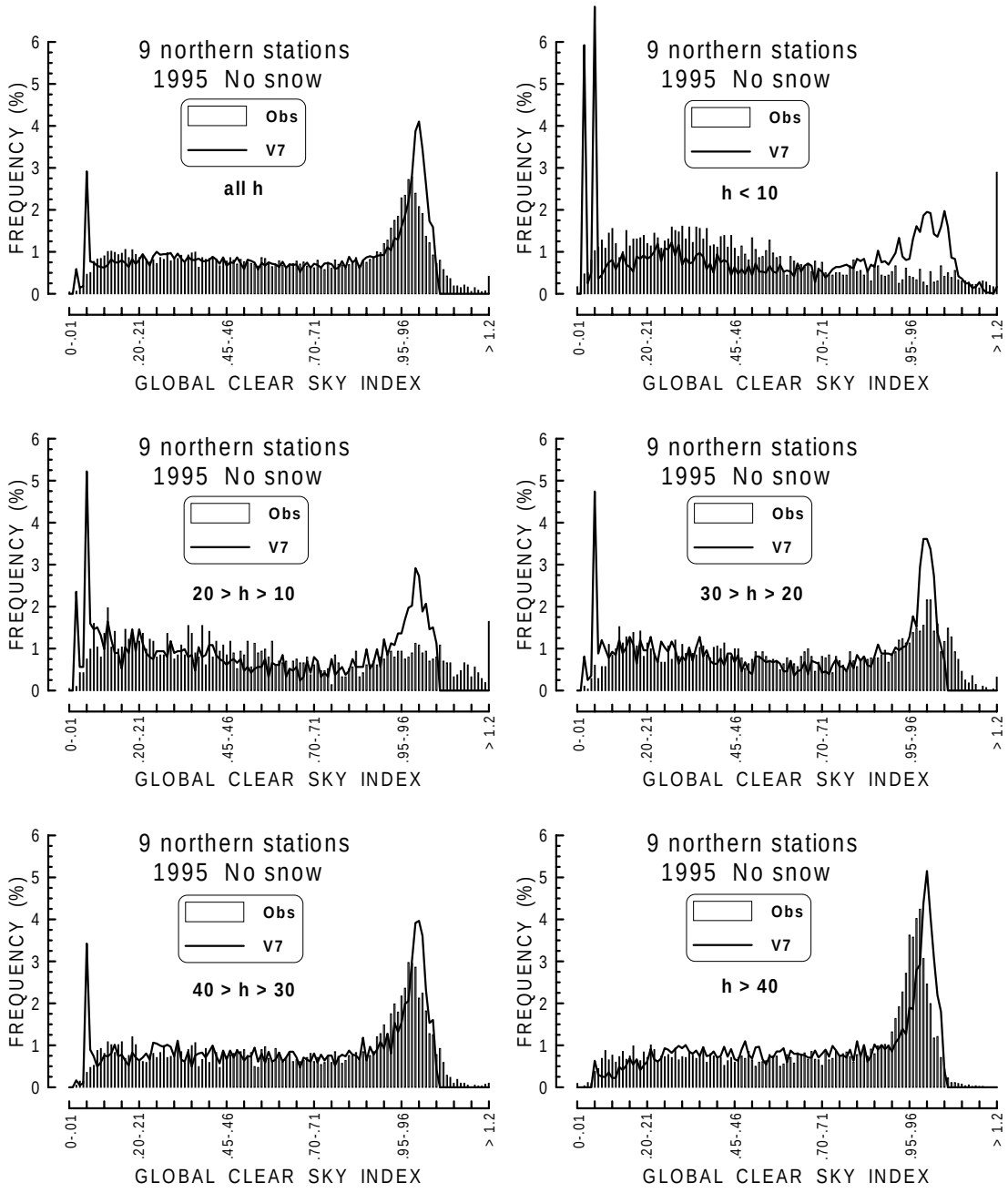

Fig. 3a) Observed (histograms) and modelled (Heliosat Version 7, curves) frequency distributions of hourly global clear sky indices for snow-free period at the 9 northern stations in Table 1 collectively, for different solar elevation (h) intervals.

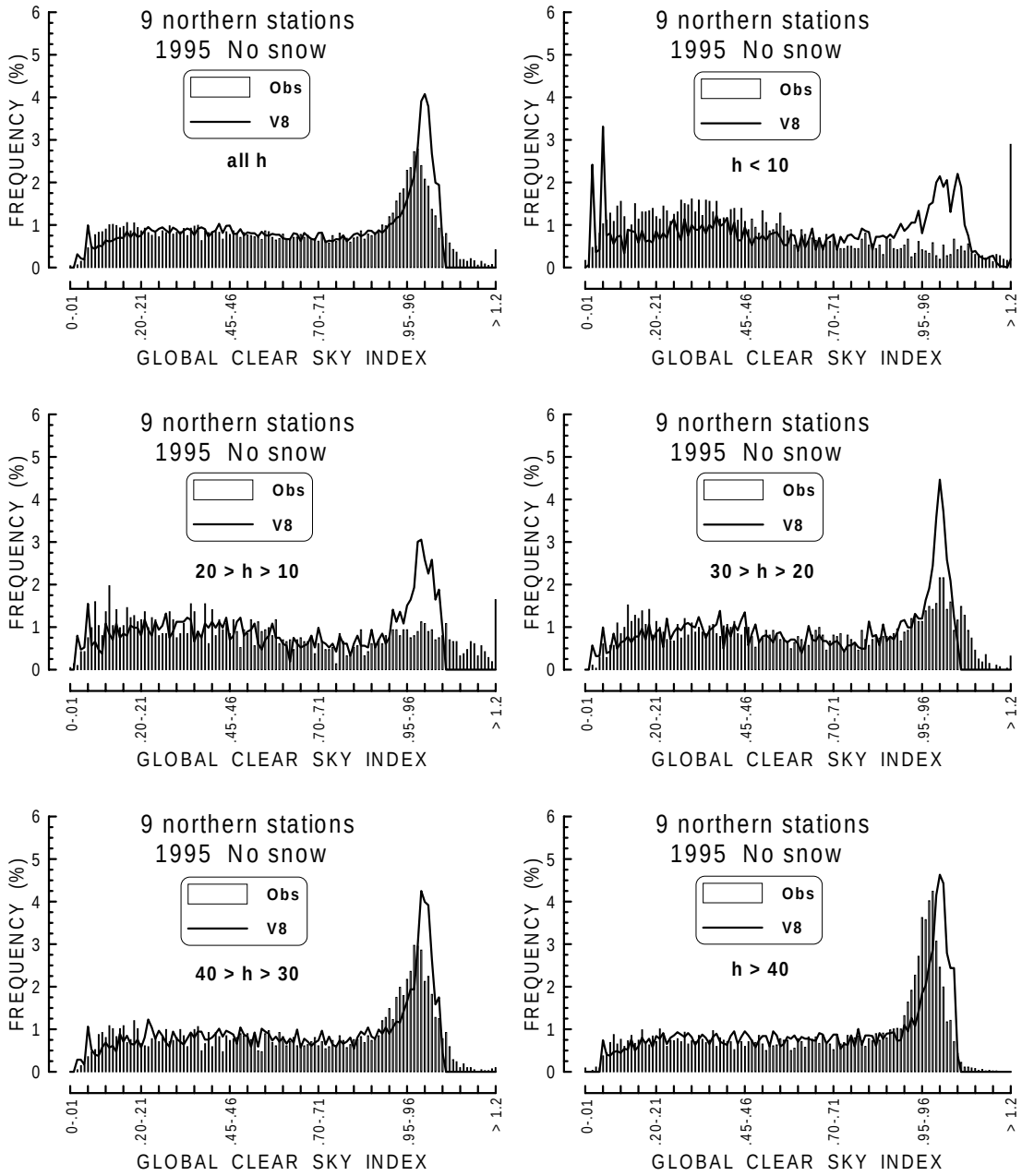

Fig. 3b) Same as Fig. 3a), but for Heliosat Version 8.

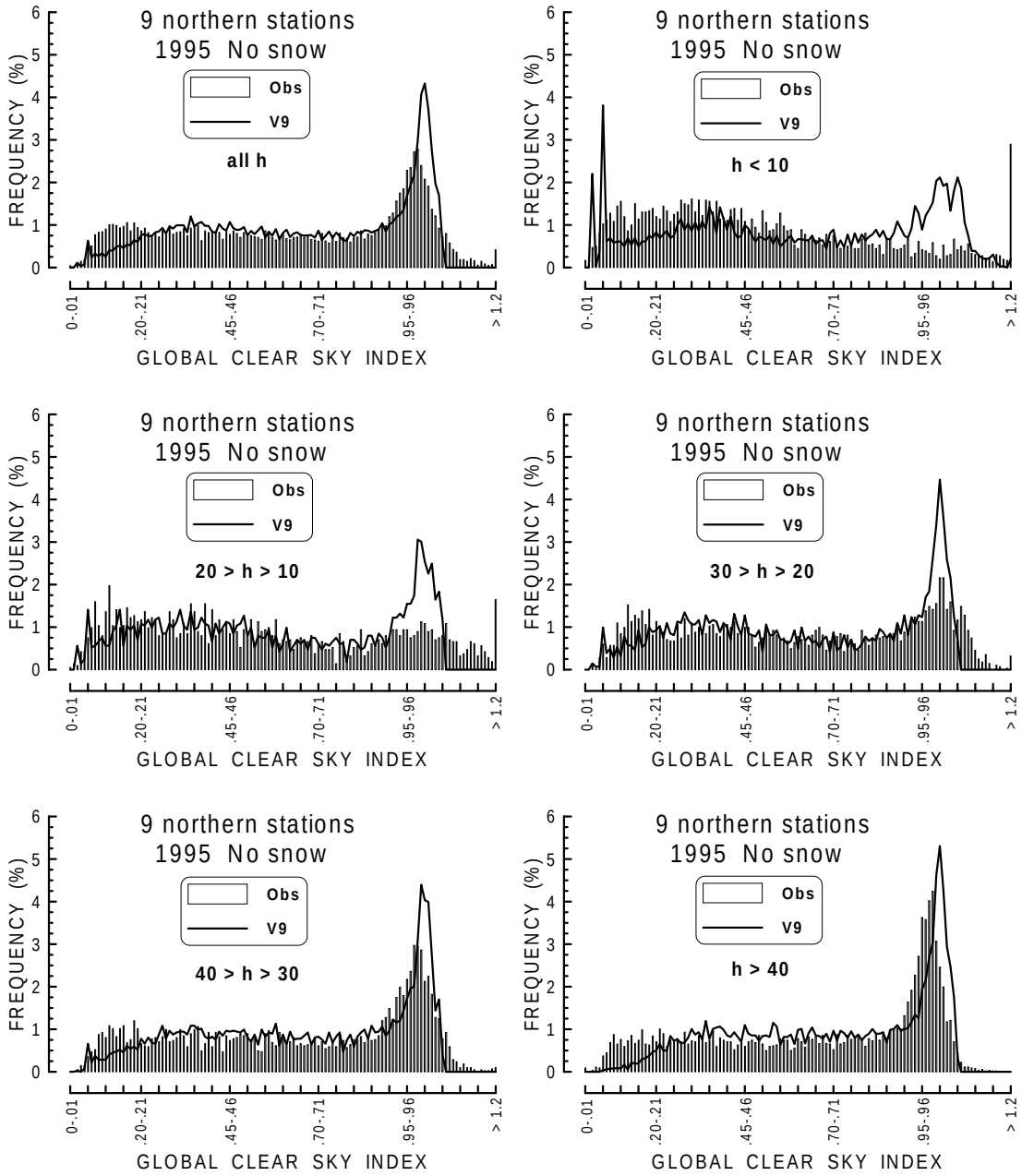

Fig. 3c) Same as Fig. 3a), but for Heliosat Version 9.

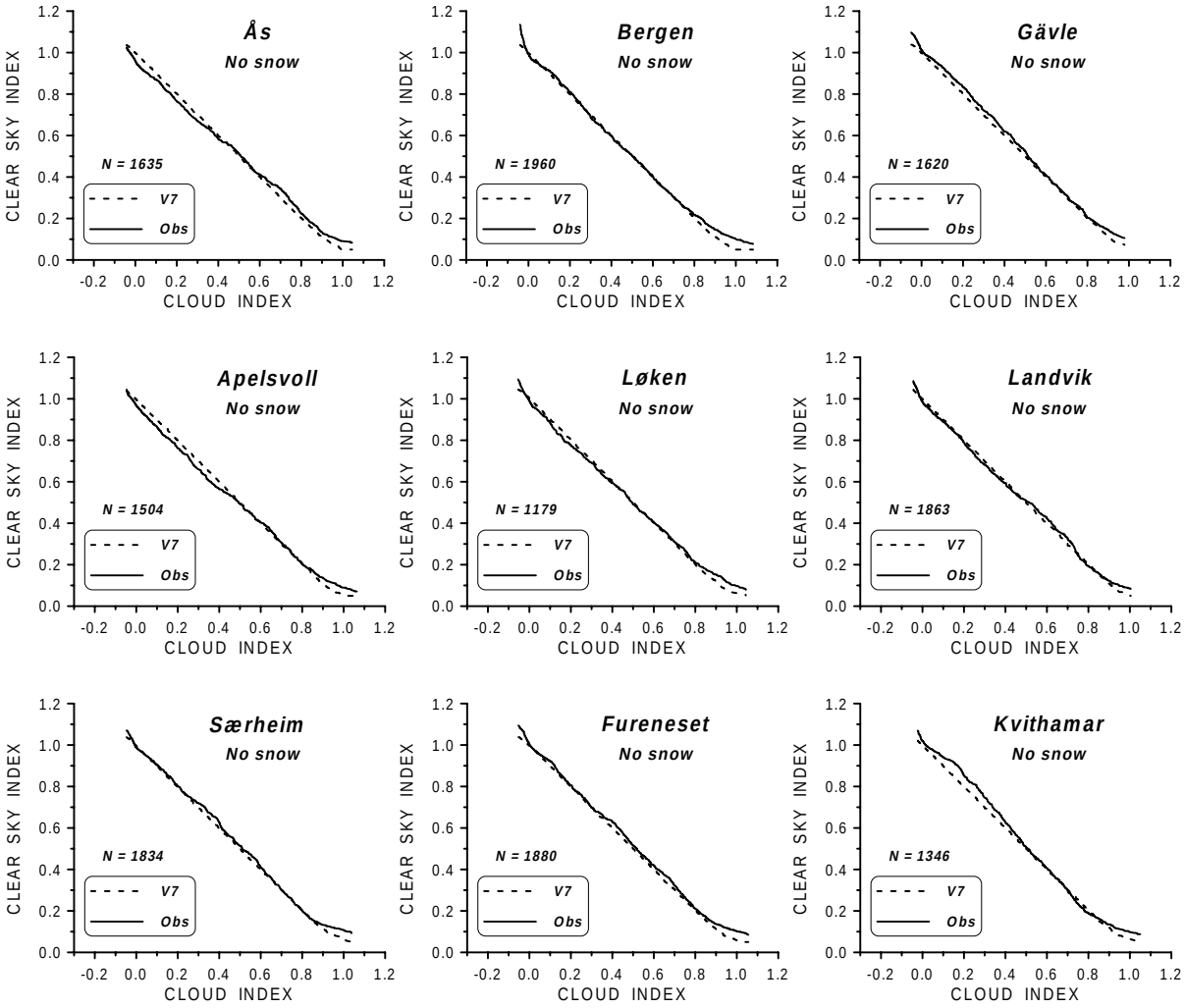

Fig. 4a) "Percentile match curves" between hourly global clear sky index (observed and modelled from Heliosat Version 7) and cloud index (modelled from Heliosat Version 7) [see text] for the snow-free period at each of the 9 northern stations in Table 1. Curves are drawn for the central 95% of the distributions. The number of hours (N) are also given.

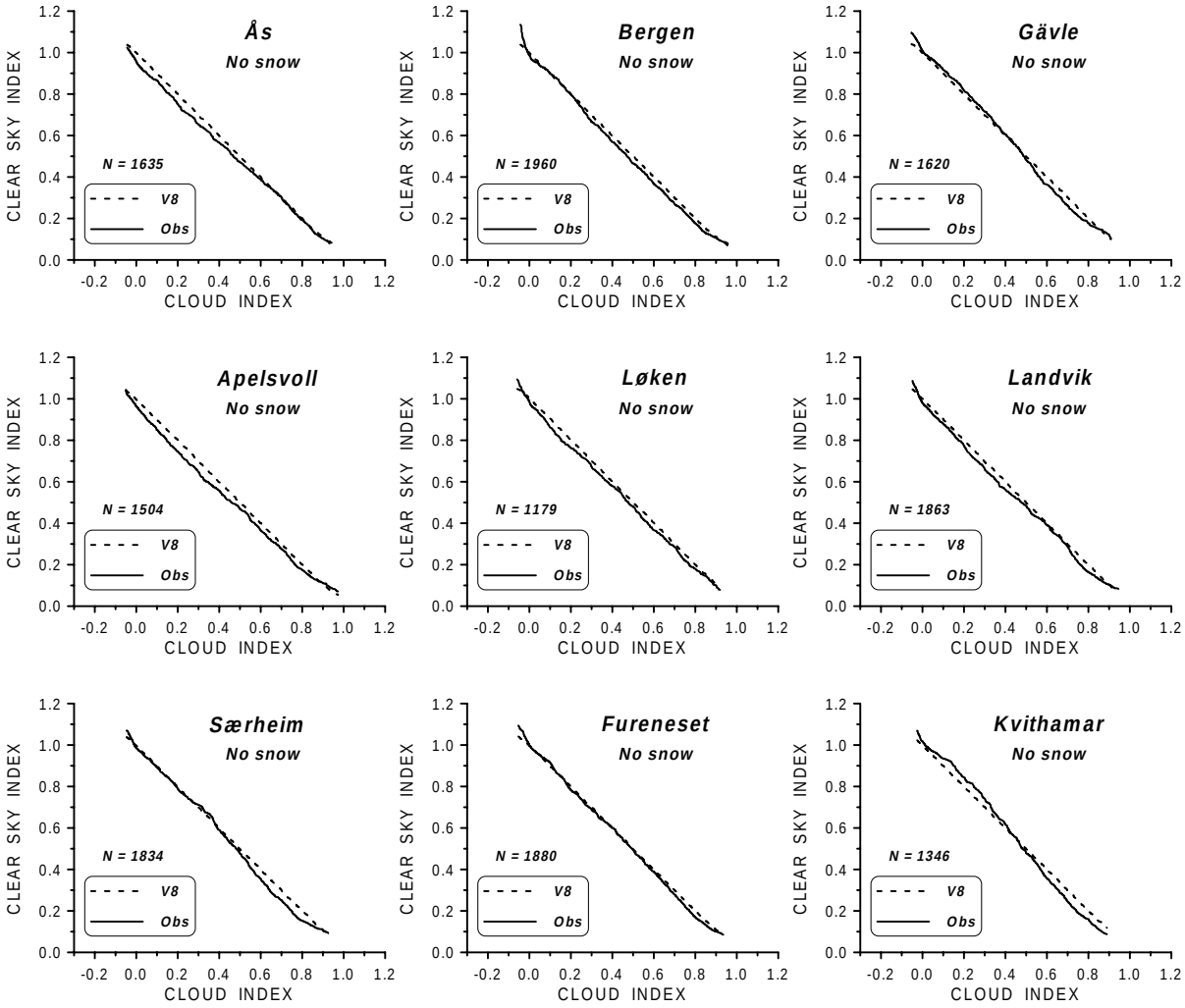

Fig. 4b) Same as Fig. 4a), but for Heliosat Version 8).

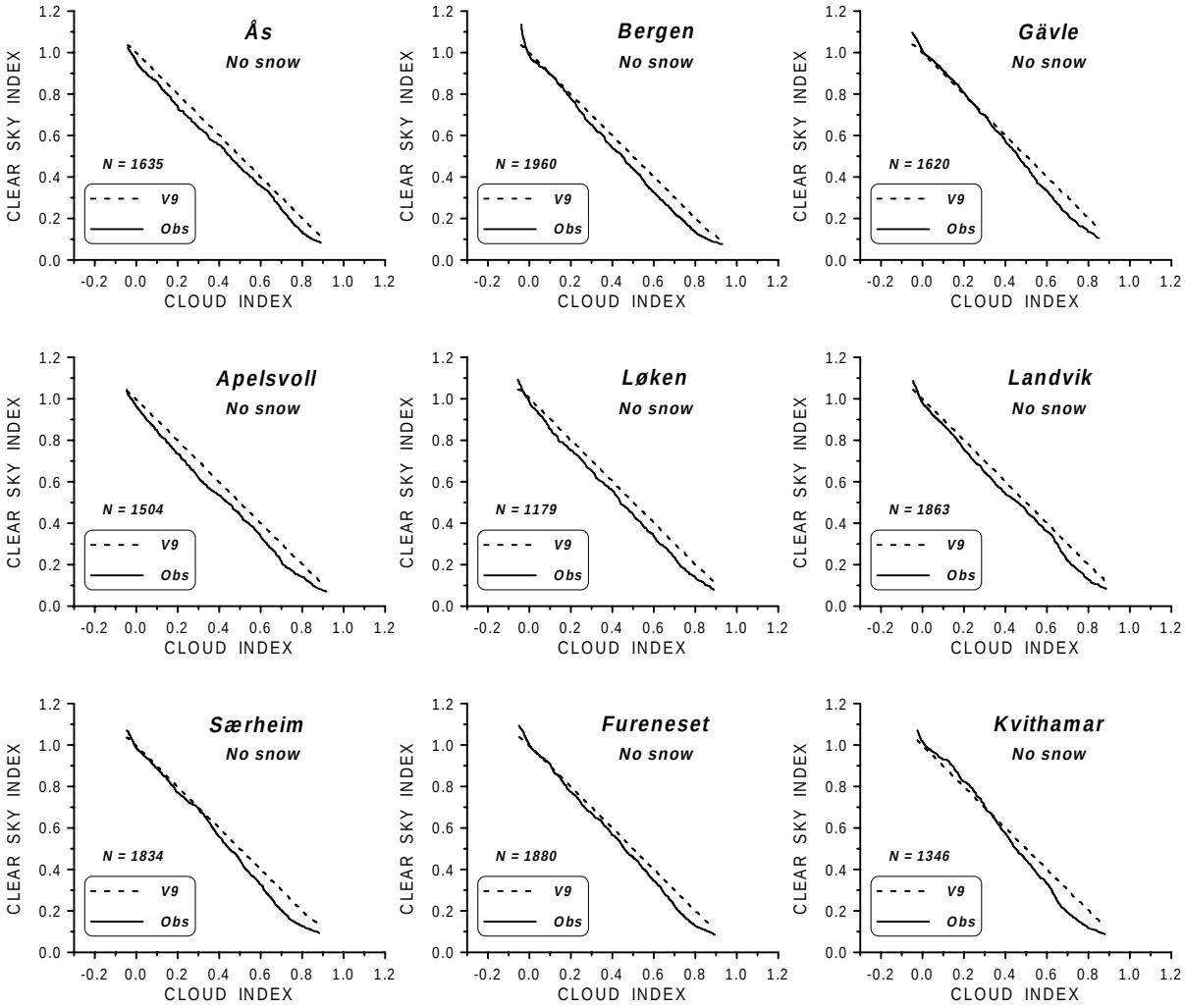

Fig. 4c) Same as Fig. 4a), but for Heliosat Version 9.

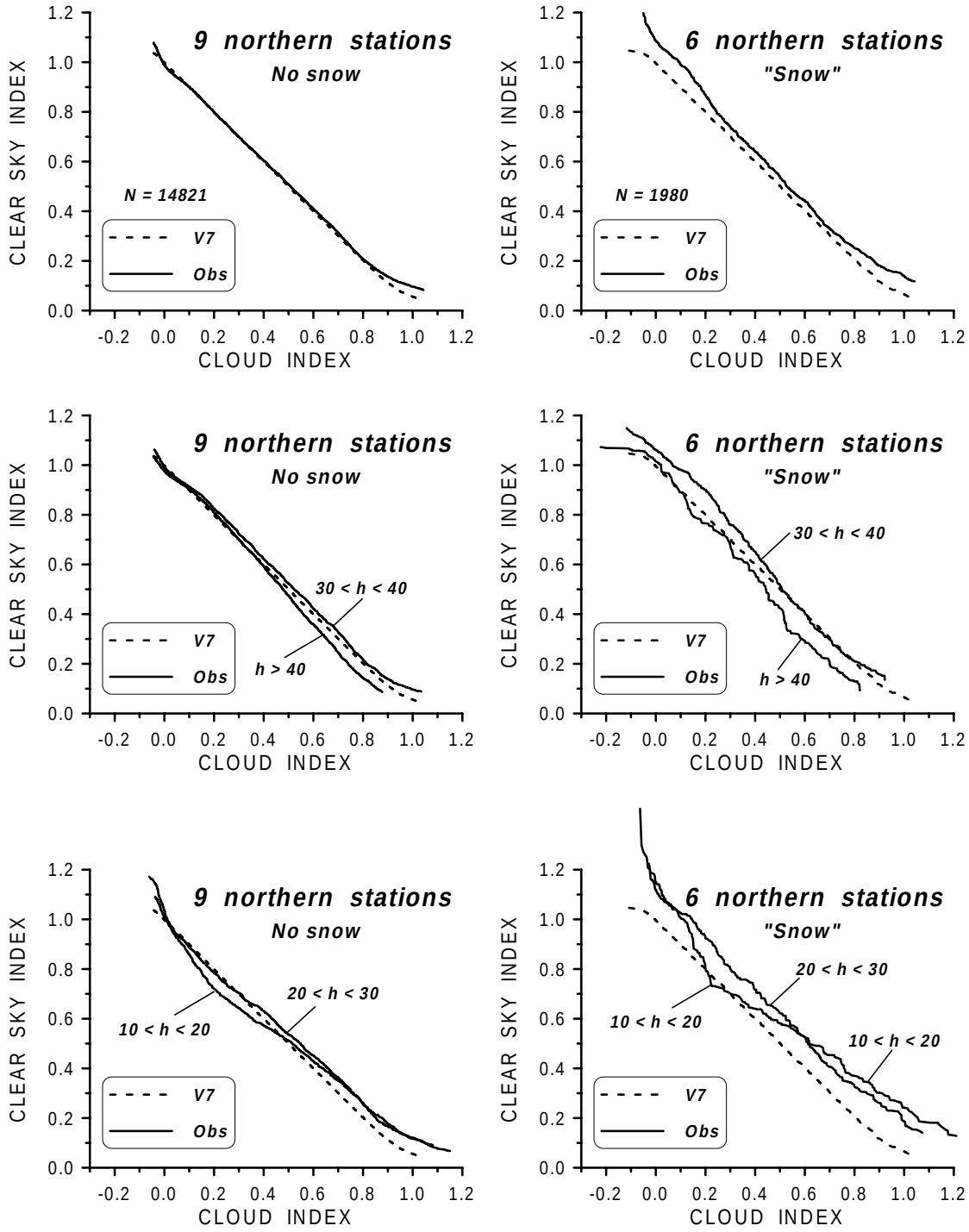

Fig. 5a) "Percentile match curves" between hourly global clear sky index (observed and modelled from Heliosat Version 7) and cloud index (modelled from Heliosat Version 7) [see text] for all hours (upper part) and for different solar elevation (h) intervals (middle and lower part) collectively for the snow-free period at the 9 stations in Table 1 (left column) and for the possibly snow affected periods at 6 stations (right column). Curves are drawn for the central 95% of the distributions.

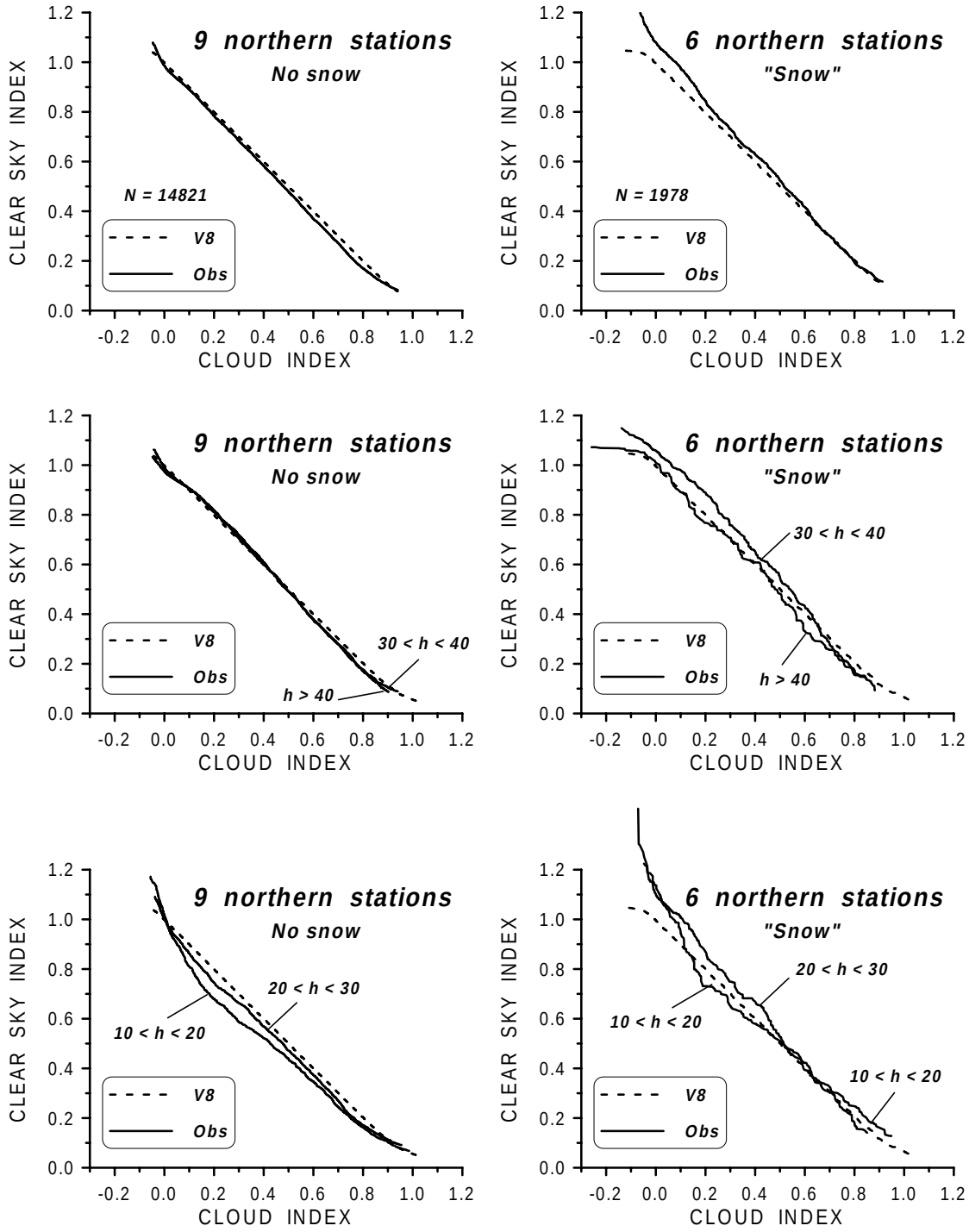

Fig. 5b) Same as Fig. 5a), but for Heliosat Version 8.

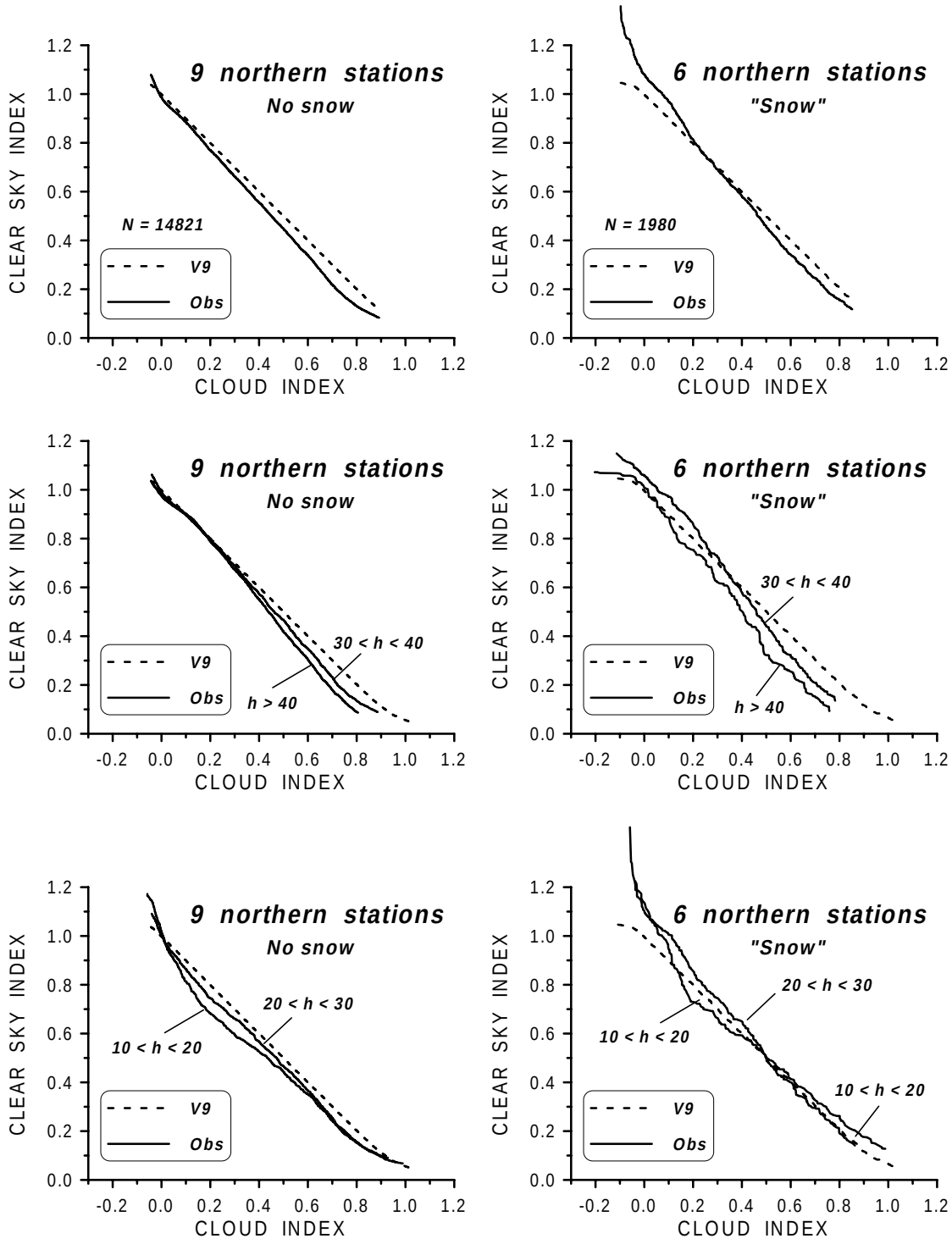

Fig. 5c) Same as Fig. 5a), but for Heliosat Version 9.

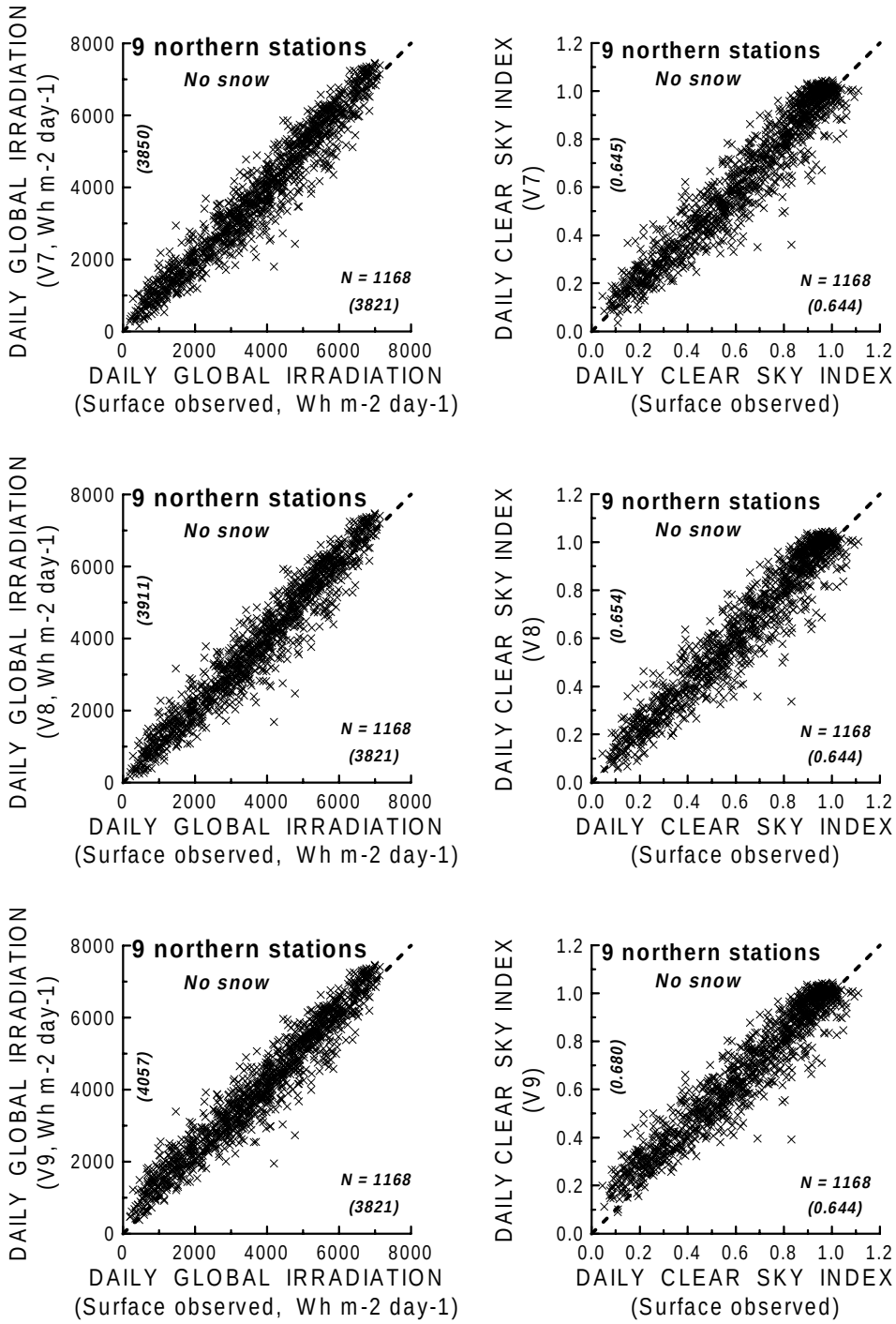

Fig. 6a) Observed daily global irradiation (left) and global clear sky index (right) plotted against Heliosat modelled values (Version 7, upper; Version 8, middle; Version 9, lower) for snow-free periods at 9 stations. The number of days (N) together with observed and modelled averages (in parentheses along the axes) are also given.

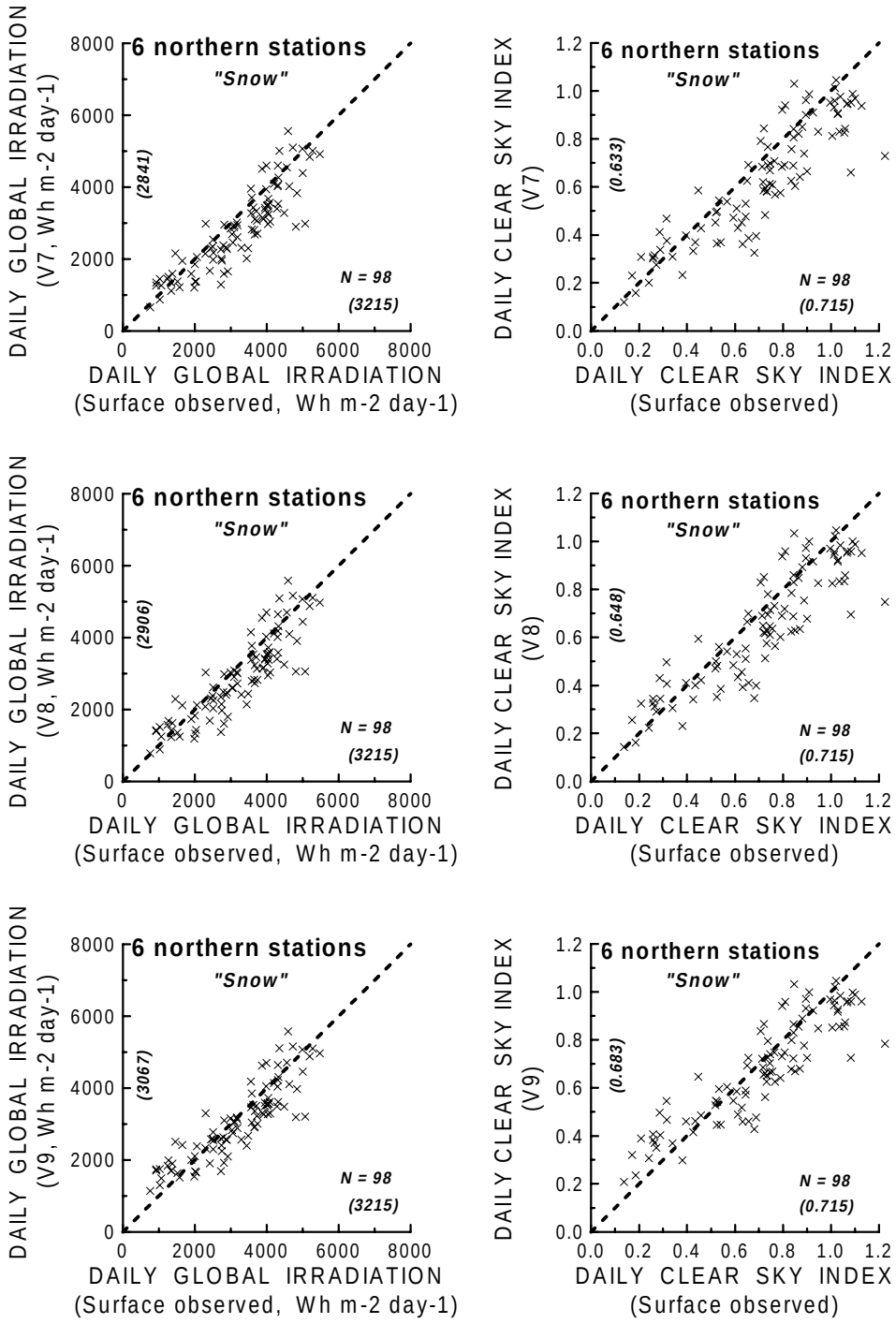

Fig. 6b) Same as Fig. 6a), but for possibly snow affected periods at 6 stations.

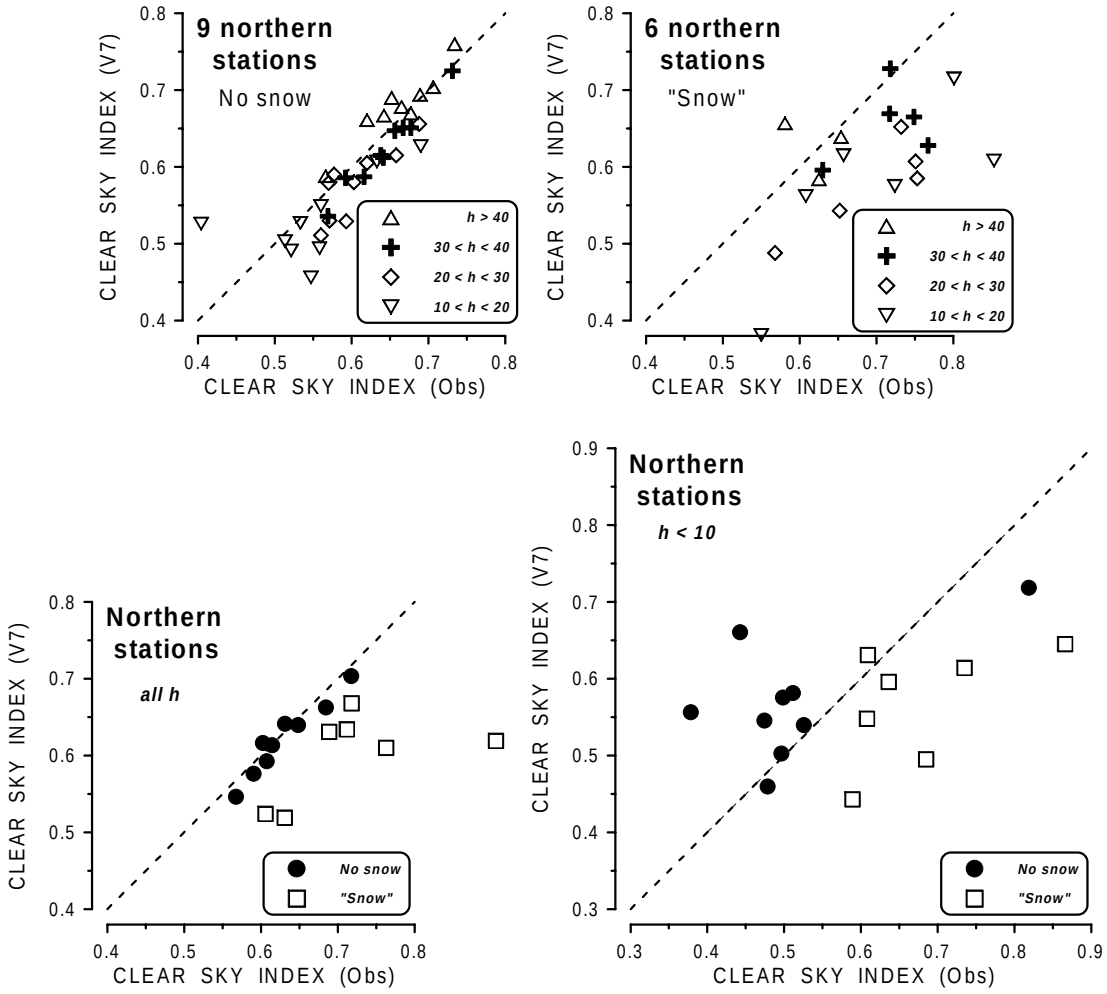

Fig. 7a) Upper part: Group mean values of observed vs modelled (Heliosat Version 7) hourly global clear sky index for different solar elevation intervals for the snow free periods at 9 northern stations (left) and for the possibly snow affected periods at 6 northern stations (right).
Lower part: Overall mean values for all hours with solar elevation above 10° (left) and below 10° (right) for each of the stations for the snow-free and the possibly snow affected periods.

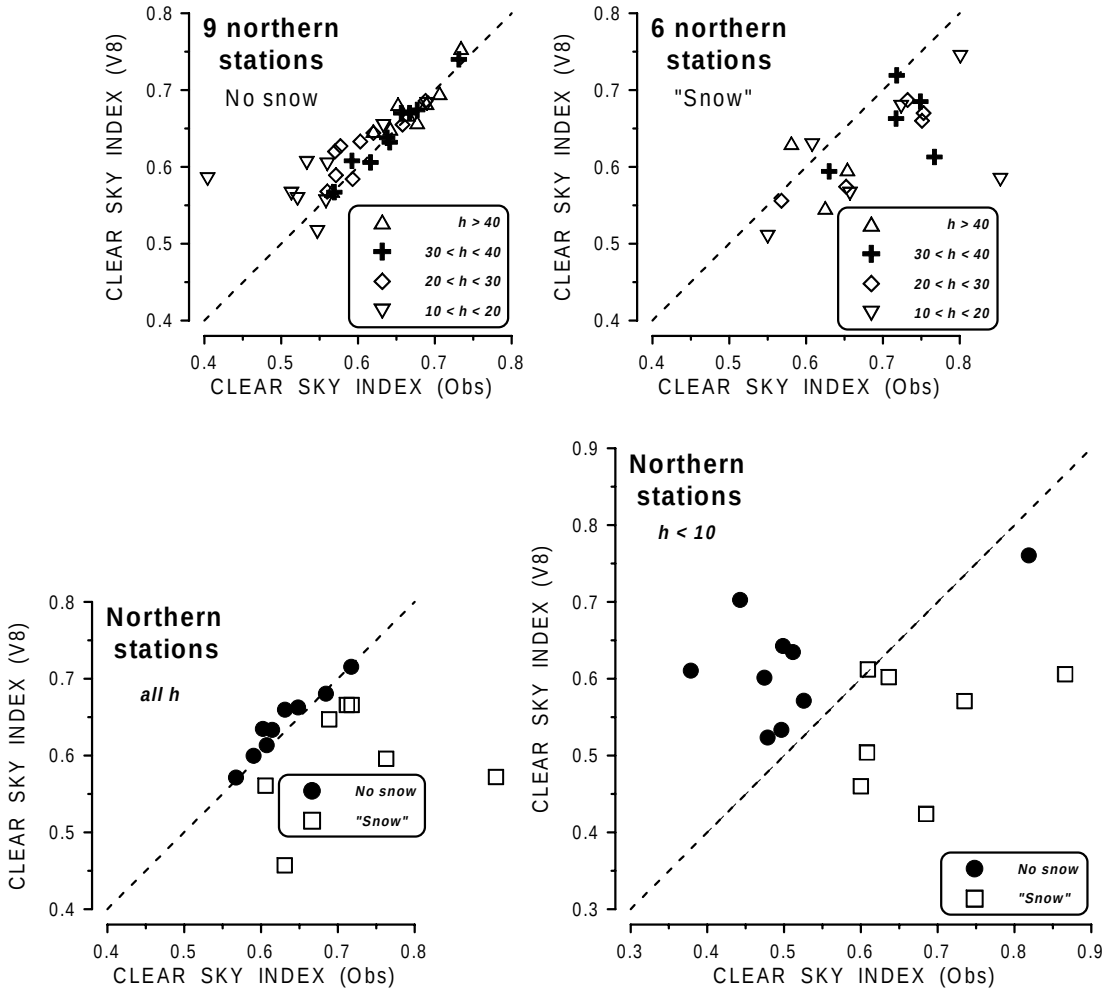

Fig. 7b) Same as Fig. 7a), but for Heliosat Version 8.

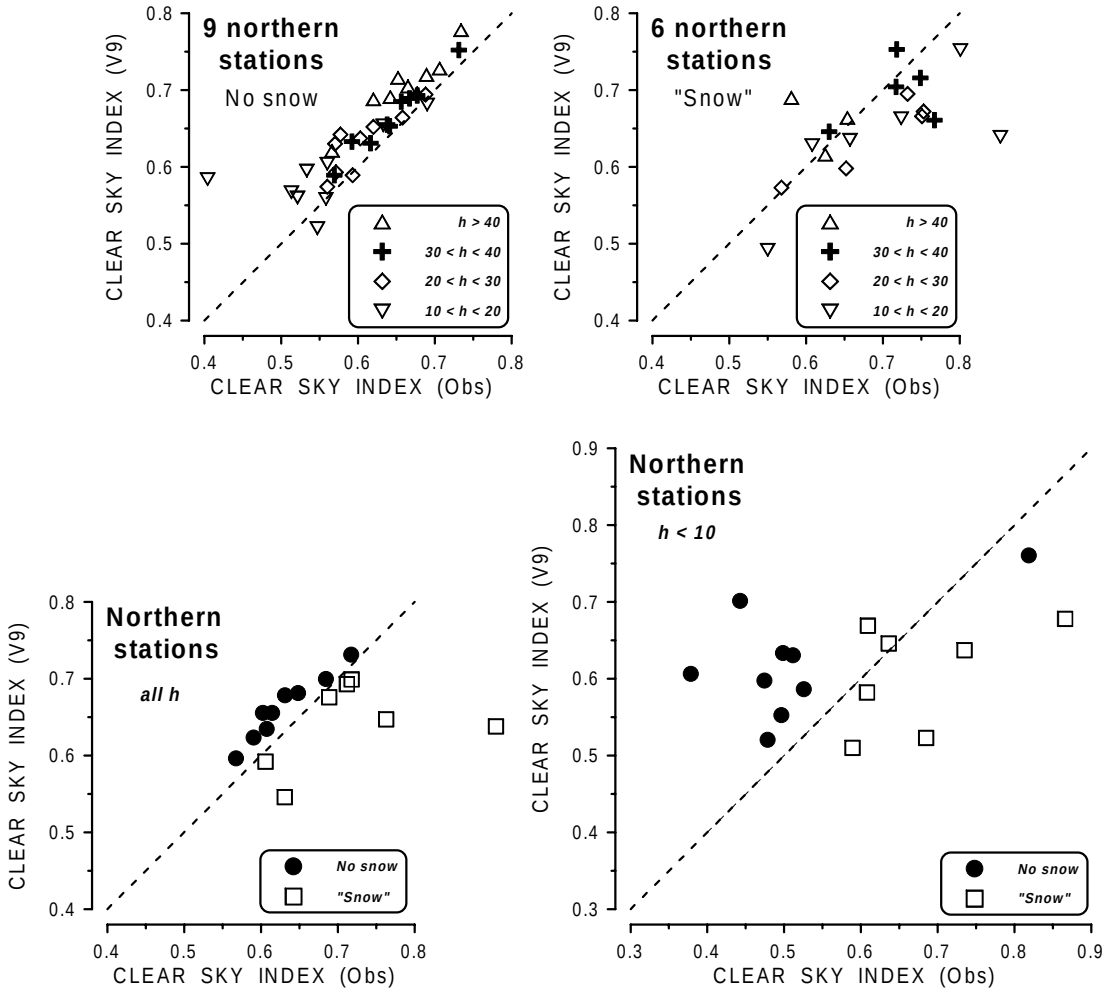

Fig. 7c) Same as Fig. 7a), but for Heliosat Version 9.

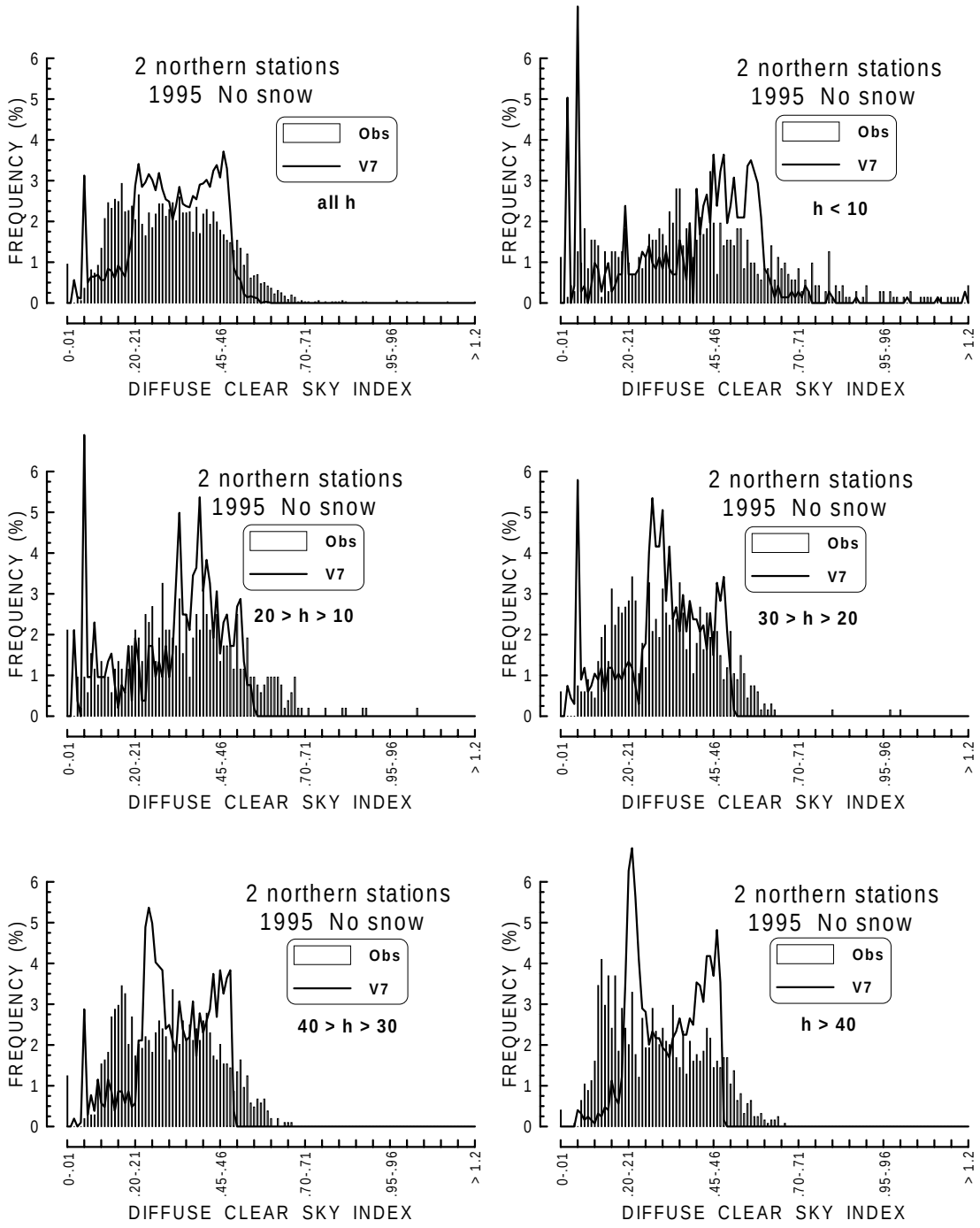

Fig. 8a) Observed (histograms) and modelled (Heliosat Version 7, curves) frequency distributions of hourly diffuse clear sky indices for snow-free period at 2 northern stations (Bergen and Gävle) for different solar elevation (h) intervals. The original Skartveit & Olseth diffuse fraction model (Skartveit & Olseth, 1987) is used for satellite derived diffuse irradiance.

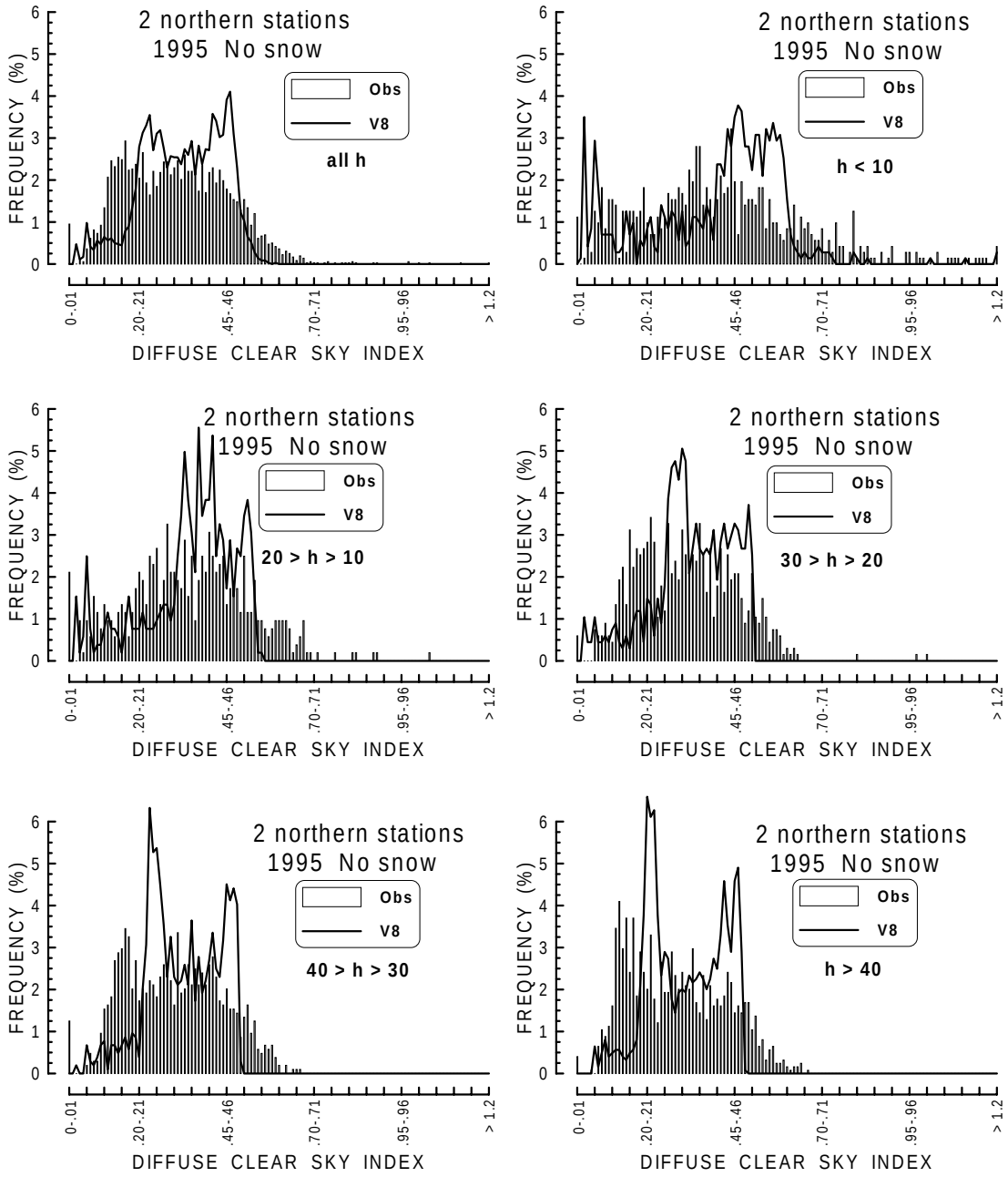

Fig. 8b) Same as Fig. 8a), but for Heliosat Version 8.

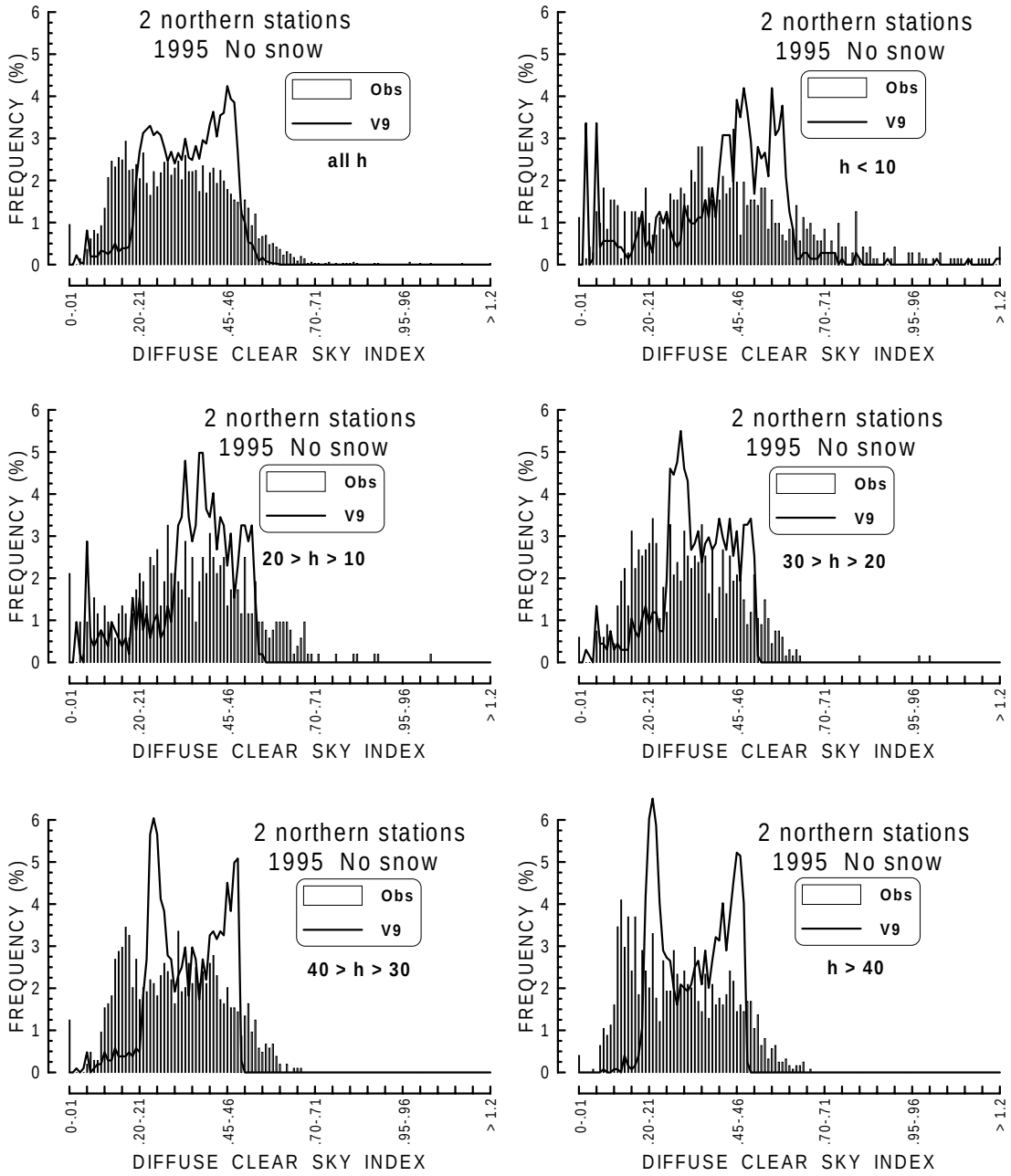

Fig. 8c) Same as Fig. 8a), but for Heliosat Version 9.

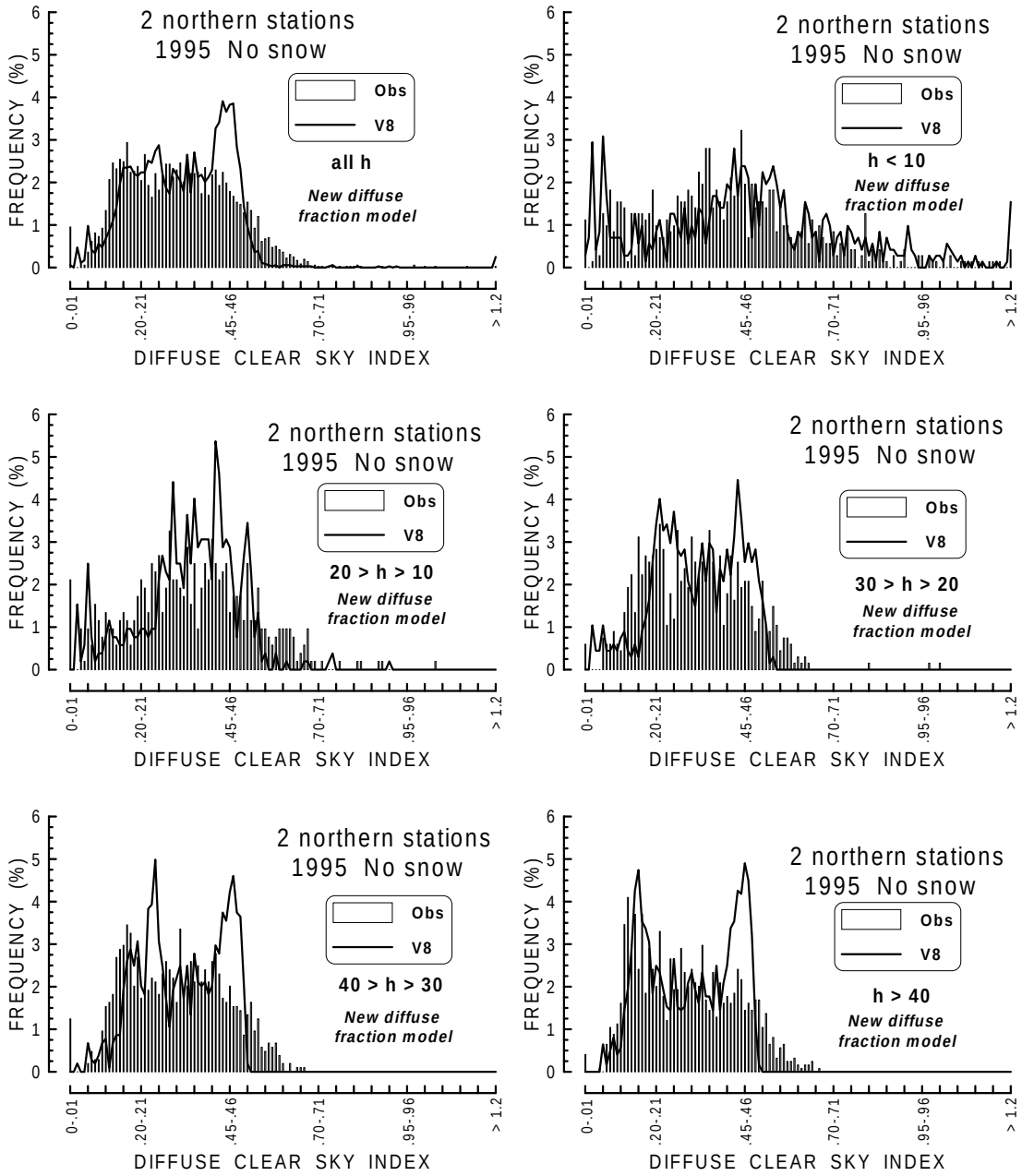

Fig. 8d) Same as Fig. 8a), but for Heliosat Version 8, with the modified diffuse fraction model (Skartveit et al., 1997).

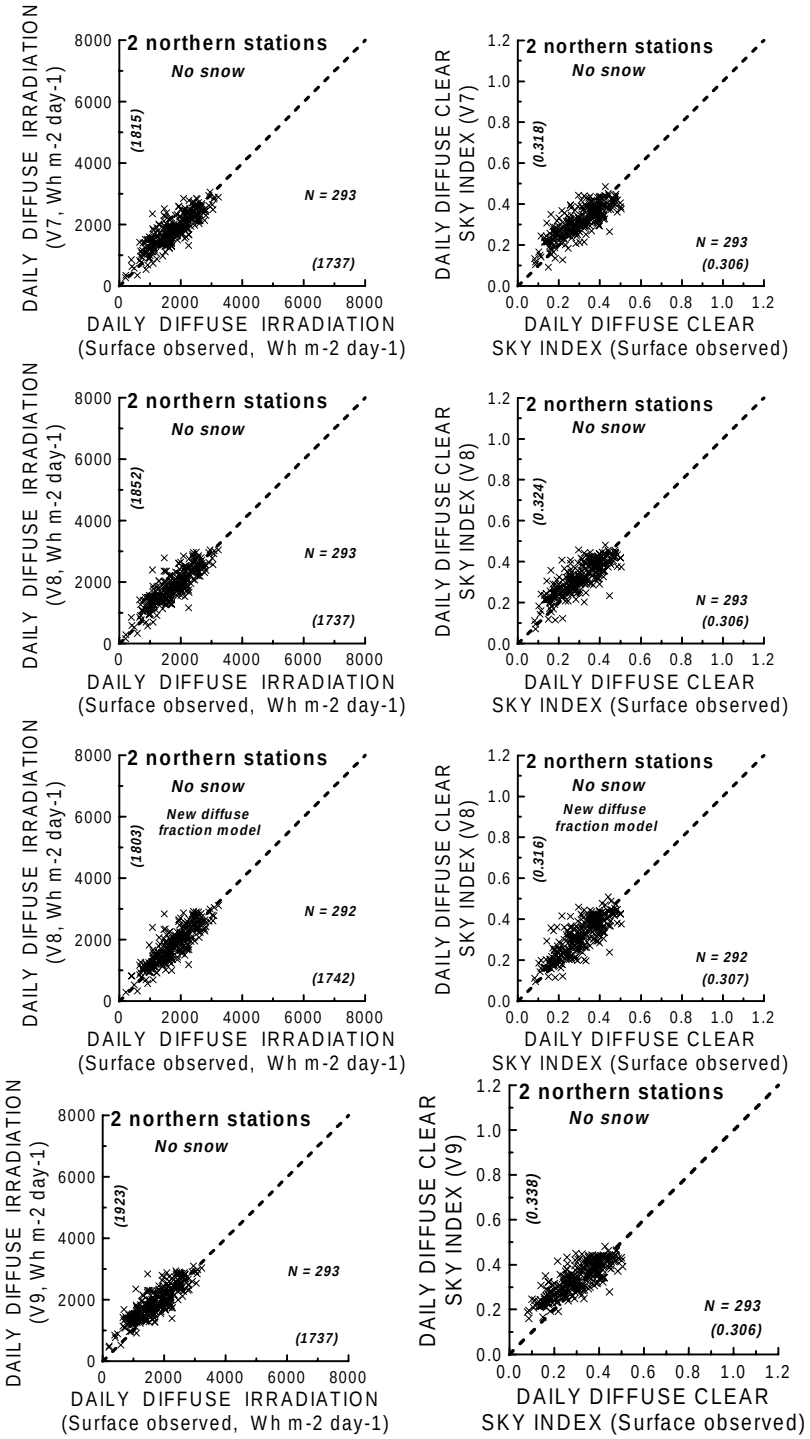

Fig. 9 Observed daily diffuse irradiation (left) and diffuse clear sky index (right) plotted against Heliosat modelled values (Version 7, upper; Version 8, middle; Version 9, lower) for snow-free periods at 2 stations. The number of days (N) together with observed and modelled averages (in parentheses along the axes) are also given. For all Versions the diffuse irradiances are estimated using the old Skartveit & Olseth diffuse fraction model (Skartveit & Olseth, 1987), but for Version 8 the modified model (Skartveit et al. 1997) is also used.

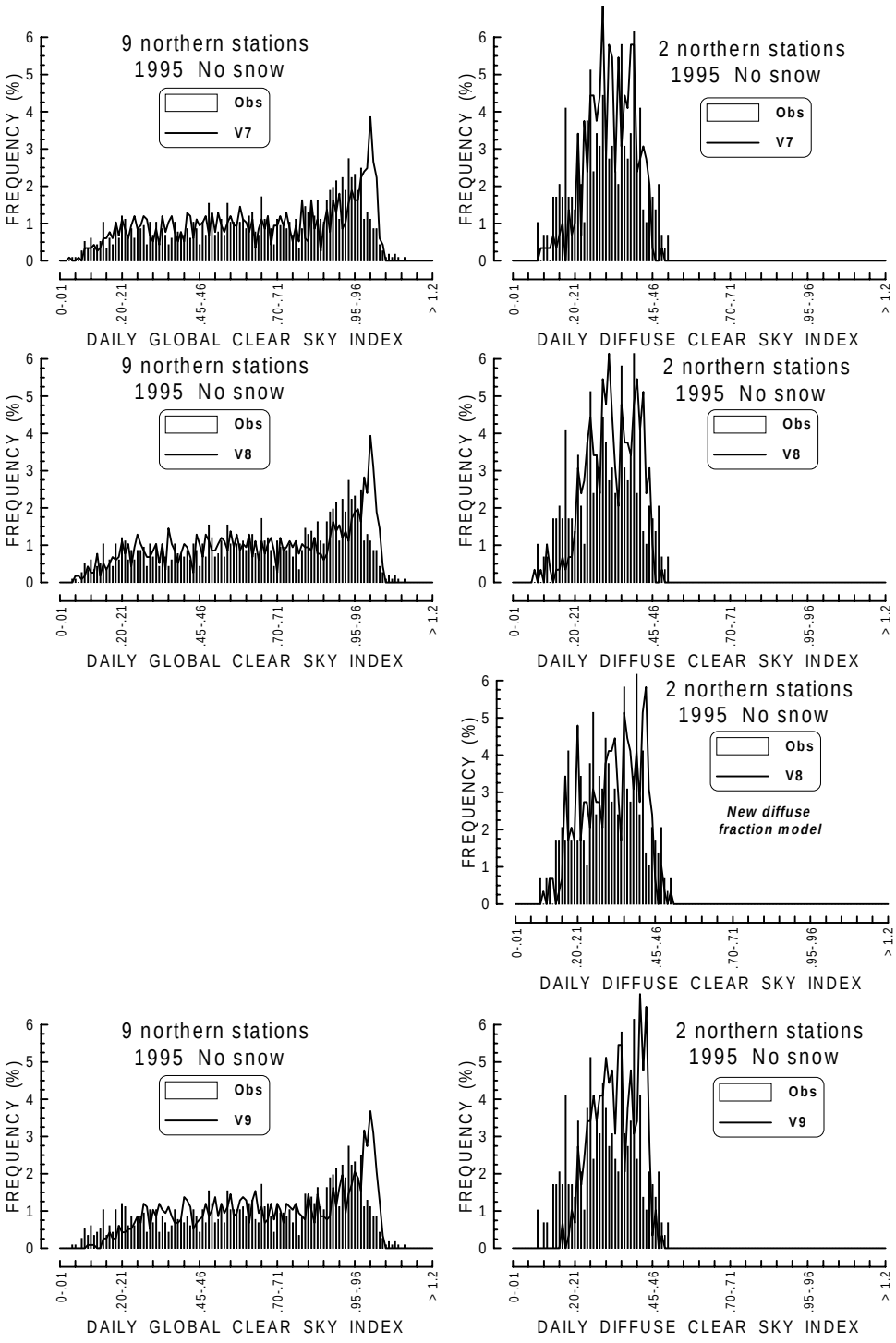

Fig. 10) Observed (histograms) and modelled (Heliosat Versions 7, upper, 8, middle, and 9, lower, curves) frequency distributions of daily global (left) and diffuse (right) clear sky indices for snow-free period at the northern stations. For all Versions the diffuse irradiances are estimated using the old Skartveit & Olseth diffuse fraction model (Skartveit & Olseth, 1987), but for Version 8 the modified model (Skartveit et al. 1997) is also used.

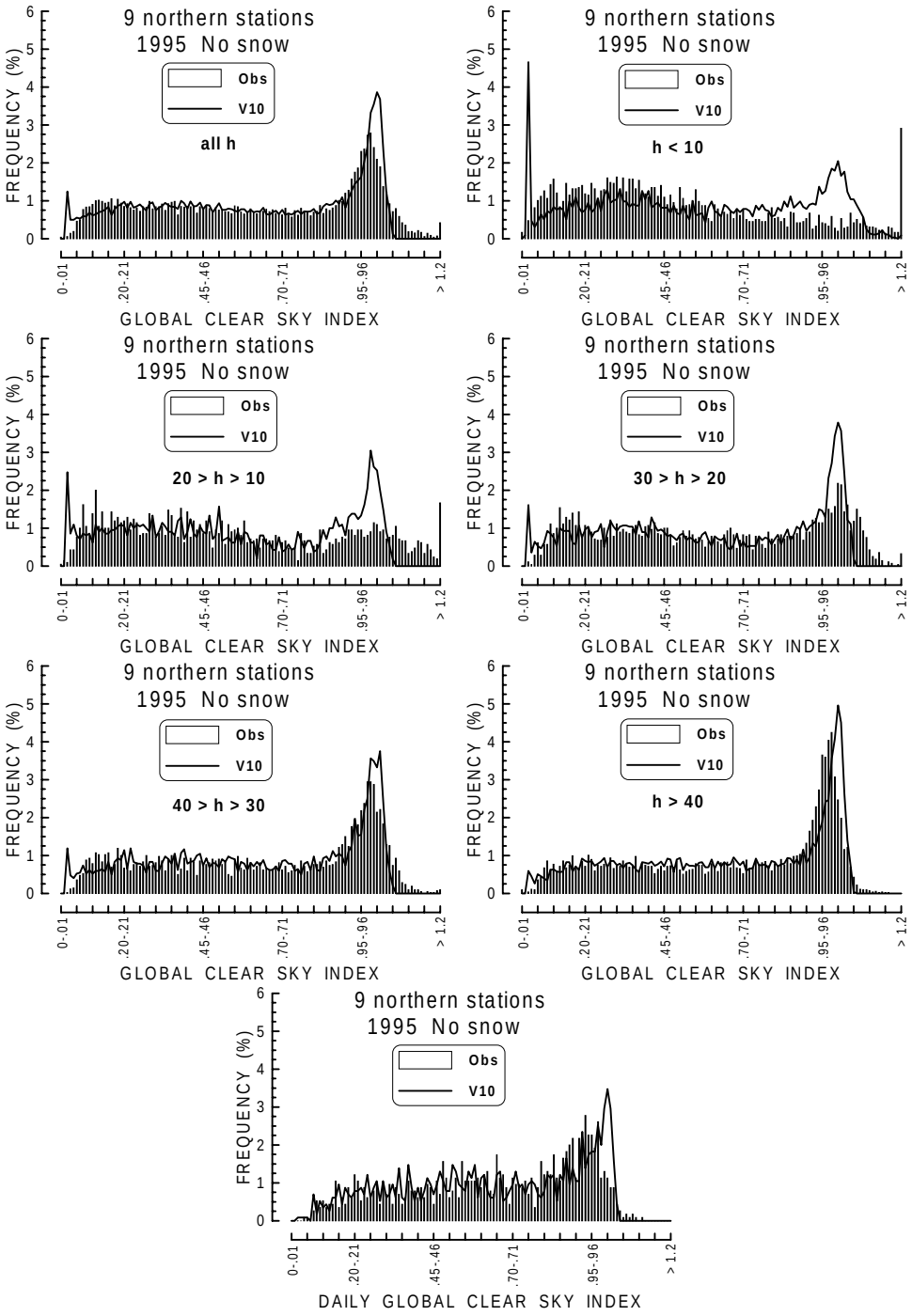

Fig. 11) Three upper rows: Observed (histograms) and modelled (Heliosat Version 10, curves) frequency distributions of hourly global clear sky indices for snow-free period at the 9 northern stations in Table 1 collectively, for different solar elevation (h) intervals. See Figs. 3a-c) for similar frequency distributions for Versions 7, 8, and 9.
Bottom: Similar frequency distributions of daily global clear sky indices for snow-free period at the 9 northern stations. See Fig. 10) for similar frequency distributions for Versions 7, 8, and 9.

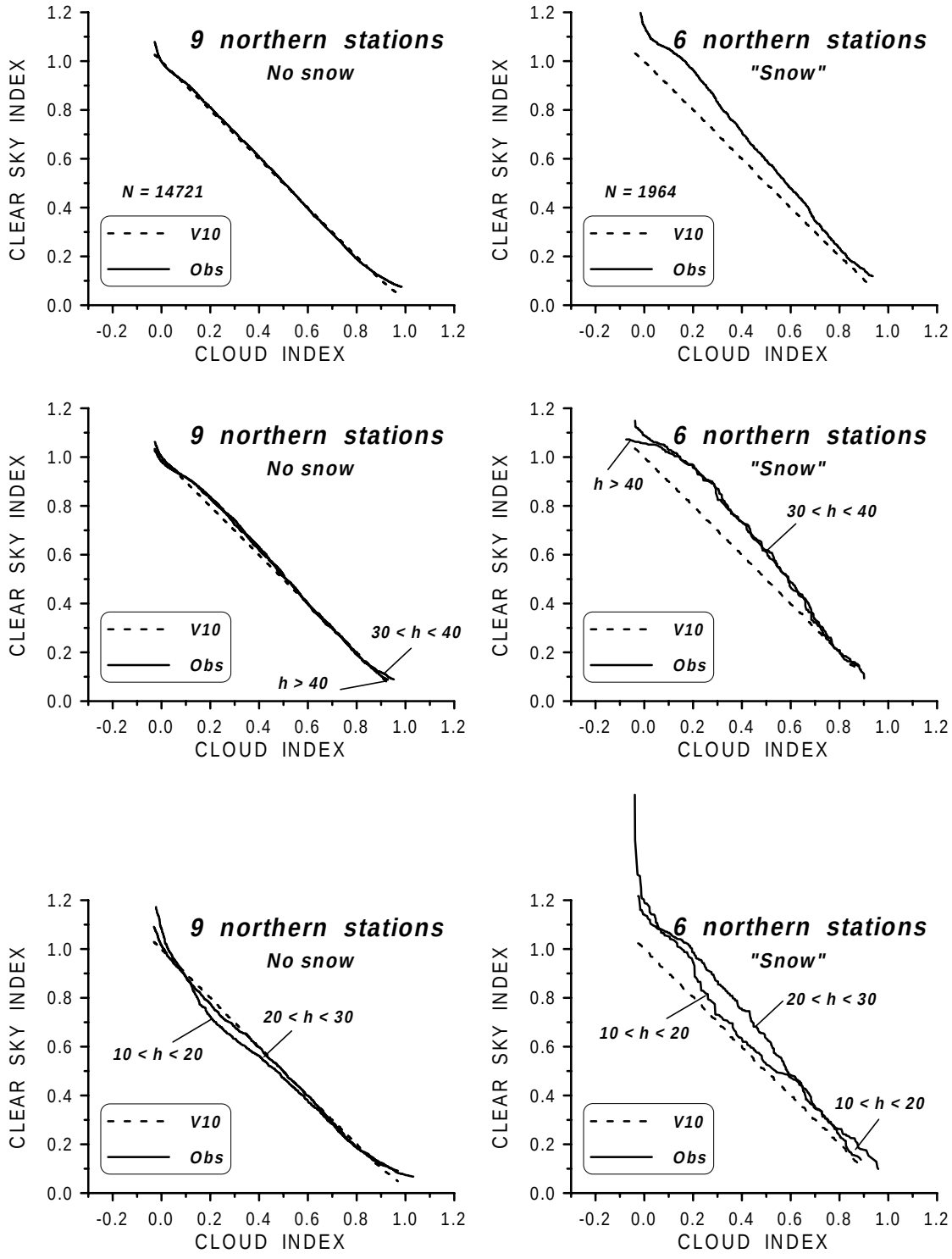

Fig. 12) "Percentile match curves" between hourly global clear sky index (observed and modelled from Heliosat Version 10) and cloud index (modelled from Heliosat Version 10) [see text] for all hours (upper part) and for different solar elevation (h) intervals (middle and lower part) collectively for the snow-free period at the 9 stations in Table 1 (left column) and for the possibly snow affected periods at 6 stations (right column). Curves are drawn for the central 95% of the distributions. See Figs. 5a-c) for similar curves for Versions 7, 8, and 9.